# Precise Point Positioning Evaluation and Airborne Lidar Calibration

Xiaohong Zhang
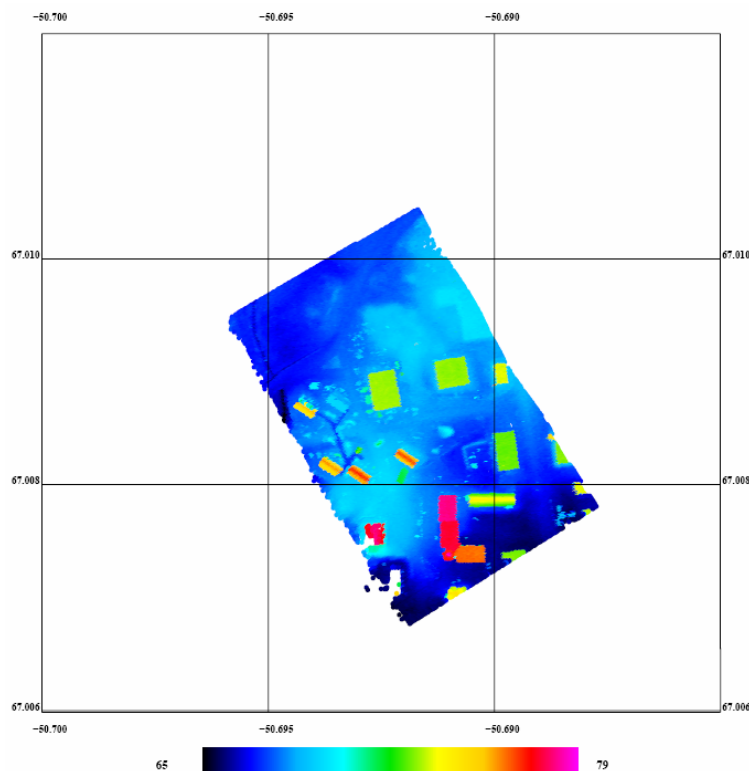
Precise Point Positioning Evaluation and Airborne Lidar Calibration

X. Zhang

Abstract

This report presents the results of investigations to determine accurate positions of aircrafts in airborne surveys (airborne gravity and airborne lidar) using precise point positioning, and also introduces a new so called "stepwise geometric misalignment determination" method to retrieve the airborne lidar system misalignment angle by automating the matching of lidar data with ground truth.

Kinematic GPS positioning has been widely used, but the available commercial software systems are normally only suitable for the short or medium range kinematic baseline. However, in polar areas, airborne surveys have baselines ranging from a few hundred kilometers to even more than one thousand kilometers due to logistic limitations. It is a challenge to the traditional kinematic GPS software based on double differenced models, such as GPSurvey or GrafNav. Since Zumberge demonstrated the perfect performance of point positioning for kinematic applications, the precise point positioning attracted a lot of attention and opened a new alternative door to kinematic positioning.

In this report different tests have been done to evaluate the ability and accuracy of the software TriP in the kinematic and static case by using internal consistency (residuals, RMS, repeatability etc.), known coordinates, ground truth and double-differenced solutions. The kinematic GPS positioning accuracy using four different software systems has been investigated and tested by comparing the degree of agreement between ground truth and the height of airborne lidar footprints derived from combining flight trajectory, orientation and lidar range. The conclusion is that the TriP software is robust and reliable, and that TriP runs much faster (10 times) than GPSurvey 2.30. A static positioning accuracy of mm to cm level could be achievable depending on the observation session length, and kinematic positioning accuracy can reach cm to dm level.

Furthermore, a new method for airborne lidar system misalignment calibration was described in detail. The proposed method was a so called 'stepwise geometric misalignment determination' based on the relationship between the point clouds on regular objects (e.g. flat top buildings) and the ground truth of the objects used for calibration. In order to extract the footprints on the objects, filtering was implemented before the calibration. Three example tests have been made and verified that the proposed method is feasible and effective.

PREFACE

This report was written to fulfill part of his visiting post-doc by Dr. Xiaohong Zhang. He came from the school of Geodesy and Geomatics, Wuhan University, China, and worked as a visiting post-doc in the Danish National Space Center for half year, under the supervision of State Geodesist Rene Forsberg. This research was supported by Danish National Space Center and Wuhan University (China).

This manuscript was edited by Nynne S. Dalå, DNSC (now KMS) for some corrections of English.

ACKNOWLEDGMENTS

- 3 -

Table of contents

1 Introduction

Kinematic GPS positioning in the post-processed or in the real-time mode is now increasingly used for many surveying and navigation applications on land, at sea and in the air. Techniques range from the robust pseudo-range-based differential GPS (DGPS) techniques capable of delivering accuracies at the meter level, to sophisticated carrier phase-based centimeter accuracy techniques, such as RTK and VRS. The distance from the mobile receiver to the nearest reference receiver may range from a few kilometers to hundreds of kilometers. A vast literature exists on the topic of airborne kinematic positioning (e.g., Cannon et al., 1992; Colombo et al., 1998; Han, 1997; Han and Rizos, 1999). However, as the distance from rover to base increases, the problems of accounting for distance-dependent biases grow in airborne kinematic positioning. For carrier phase-based techniques reliable ambiguity resolution becomes an even greater challenge. In order to derive reliable and accurate estimates of the trajectory of a survey aircraft without the establishment of dense GPS base stations, four approaches have been used as Castleden et al (2004) and Mostafa (2005) summarized: The first approach is to make use of data available from existing Continuously Operating Reference Stations (CORS) networks to estimate the position of the aircraft. While such stations are often at a considerable distance from the survey area (e.g. 50 to 500 km), they are often large in number and their data is usually freely available. More experience and results are required to make a definitive statement about using CORS data without at least one dedicated base stations, certainly the potential is there (Mostafa, 2005). The second approach is using the virtual reference station (VRS) concept. The VRS approach can deliver single coordinate accuracies of a few centimeters for a network of reference stations separated by only 50-70 km presently. The third approach is using the satellite-based differential corrections available in real-time, but only sub-meter positioning over most land areas worldwide can be achievable, an example of these systems is the NavCom. The fourth approach is using the IGS products, where the precise orbits and the satellite clock corrections are obtained after the fact and used in a single point positioning mode. Since Zumberge et al (1997) demonstrated that sub-decimeter level accuracy could be achieved using precise point positioning technology in kinematic case irrespective of baseline length. Precise point positioning is now attracting much attention internationally (Kouba, 2000; Gao, 2001, Bisnarth et al., 2002, Columbo, 2004). Importantly, it requires only one dual-frequency carrier-phase GPS receiver and thus avoids the expense and logistics of deploying a network of GPS receivers surrounding the area of interest, as is needed for the MRS and VRS techniques. It seems that precise point positioning opens a new alternative way to long range kinematic positioning. In the following chapters, details about precise point positioning and its application in airborne survey will be given. The focus in this report is evaluation of the precise point positioning accuracy using the TriP program developed by the Author.

2 Precise Point Positioning

2.1 IGS organization and its data and products

The International GNSS Service (IGS), formerly the International GPS Service, is a voluntary federation of more than 200 worldwide agencies that pool resources and permanent GPS & GLONASS station data to generate precise GPS & GLONASS products (figure 2.1). The IGS is committed to provide the highest quality data and products as the standard for Global Navigation Satellite Systems (GNSS) in support of Earth science research, multidisciplinary applications, and education. Currently the IGS includes GPS and the Russian GLONASS, and intends to incorporate future GNSS. One can think of the IGS as the highest-precision international civilian GPS community.
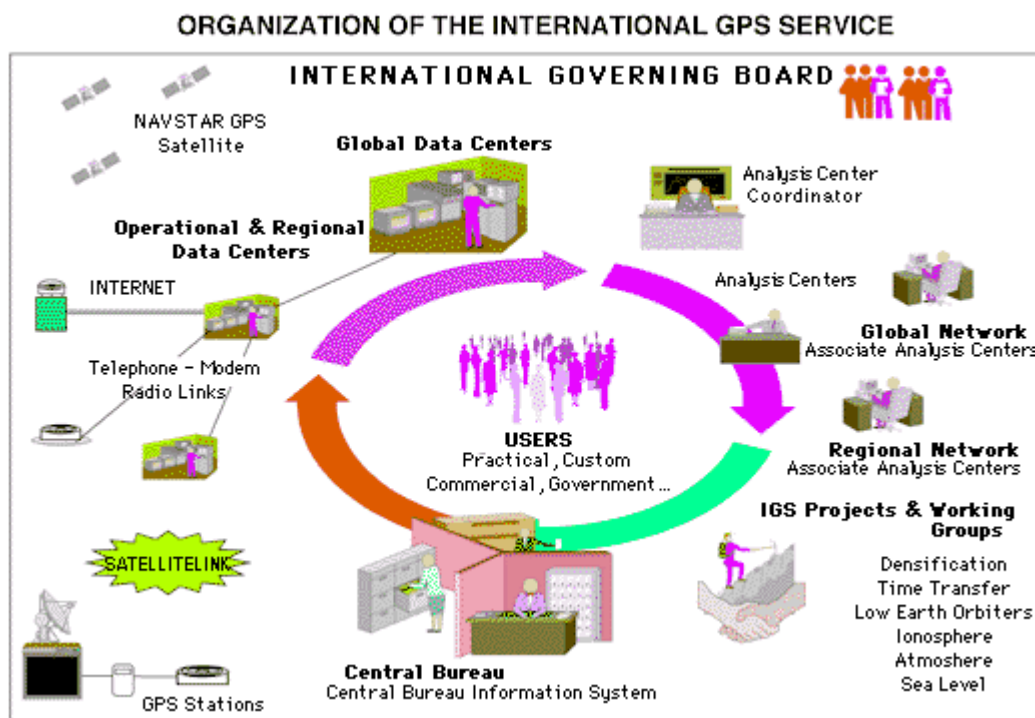
Fig 2.1 Organization of the IGS

The IGS collects, archives, and distributes GPS observation data sets of sufficient accuracy to meet the objectives of a wide range of scientific and engineering applications and studies (table 2.1). These data sets are used to generate the following products:

- ❖ GPS and GLONASS satellite ephemerides
- ❖ Earth rotation parameters
- ❖ IGS tracking station coordinates and velocities
- ❖ GPS satellite and IGS tracking station clock information
- ❖ Zenith tropospheric path delay estimates
- ❖ Global ionospheric maps

IGS products support scientific activities such as improving and extending the International Terrestrial Reference Frame (ITRF) maintained by the International Earth Rotation and Reference Systems Service (IERS), monitoring deformations of

the solid Earth and variations in the liquid Earth (sea level, ice sheets, etc.) and in Earth rotation, determining orbits of scientific satellites, and monitoring the troposphere and ionosphere. (Please go to http://igscb.jpl.nasa.gov/ if you want know more about IGS)

Fig.2.2 IGS Global network

Tab.2.1 IGS GPS data table

IGS Ground GPS Data Table				
	Latency	**Updates**	**Sample Interval**	**Archive locations**
GPS	~1 day	Daily	30 sec	CDDIS(US-MD) SOPAC(US-CA) IGN(FR)
	~1 hour	hourly	30 sec	CDDIS(US-MD) SOPAC(US-CA) IGN(FR)
	~15 min	15 min	1 sec(*)	CDDIS(US-MD)
	(*) Note: Selected subhourly stations have sampling intervals 1 sec < t < 10 sec)			
GPS Broadcast ephemerides	~1 day	Daily		CDDIS(US-MD) SOPAC(US-CA) IGN(FR)
	~1 hour	hourly		CDDIS(US-MD) SOPAC(US-CA) IGN(FR)
	~15 min	15 min		CDDIS(US-MD)

Tab. 2.2 GPS Satellite Ephemerides/Satellite & Station Clocks products

IGS Product Table [GPS Broadcast values included for comparison]						
		Accuracy	**Latency**	**Updates**	**Sample Interval**	**Archive locations**
GPS Satellite Ephemerides/ Satellite & Station Clocks						
Broadcast	orbits	~200 cm	real time	--	daily	CDDIS(US-MD) SOPAC(US-CA) IGN(FR)
	Sat. clocks	~7 ns				
Ultra-Rapid (predicted half)	orbits	~10 cm	real time	four times daily	15 min	CDDIS(US-MD) SOPAC(US-CA) IGN(FR) IGS CB(US-CA)
	Sat. clocks	~5 ns				
Ultra-Rapid (observed half)	orbits	<5 cm	3 hours	four times daily	15 min	CDDIS(US-MD) SOPAC(US-CA) IGN(FR) IGS CB(US-CA)
	Sat. clocks	~0.2 ns				
Rapid	orbits	<5 cm	17 hours	daily	15 min	CDDIS(US-MD) SOPAC(US-CA) IGN(FR) IGS CB(US-CA)
	Sat. & Stn. clocks	0.1 ns			5 min	
Final	orbits	<5 cm	~13 days	weekly	15 min	CDDIS(US-MD) SOPAC(US-CA) IGN(FR) IGS CB(US-CA)
	Sat. & Stn. clocks	<0.1 ns			5 min	
Note 1: IGS accuracy limits, except for predicted orbits, based on comparisons with independent laser ranging results. The precision is better. Note 2: The accuracy of all clocks is expressed relative to the IGS timescale, which is linearly aligned to GPS time in one-day segments.						

2.2 Precise point positioning principle

By using the IGS precise orbit products and precise satellite clock information as the known information, and combining the GPS carrier phase and pseudo-range data, geodetic users achieve precise positioning with single dual-frequency receiver anywhere on the Earth. The method is called precise point positioning, abbreviated as PPP. In PPP, the following ionosphere-free combined observations are generally used to form the observation equations.

$$l_P = \rho + c(dt - dT) + M \cdot zpd + \varepsilon_P \qquad (2\text{-}1)$$

$$l_\Phi = \rho + c(dt - dT) + amb + M \cdot zpd + \varepsilon_P \qquad (2\text{-}2)$$

where: l_P is code ionosphere-free combination of P1 and P2 ; l_Φ is phase ionosphere-free combination of L1 and L2 ; dt is the receiver clock offset ; dT is the satellite clock offset ; c is the light velocity ; amb is ambiguity of the phase ionosphere-free combination(non-integer) ; M is the mapping function; zpd is the zenith tropospheric delay correction; ε_P and ε_Φ are noise of combined observations ; ρ is geometric range between receiver (X_r, Y_r, Z_r) and satellite (X_S, Y_S, Z_S) :

$$\rho = \sqrt{(X_S - X_r)^2 + (Y_S - Y_r)^2 + (Z_S - Z_r)^2}$$

Linearization of observation equations (1) and (2) around the a-priori parameters (X_0) and observations equation becomes, in matrix form:

$$V = A\delta X + W$$

Where A is the design matrix; δX is the vector of corrections to the unknown parameters (X) included receiver position, receiver clock offset, ambiguity of the phase ionosphere-free combination and zenith tropospheric delay correction; W is the misclosure vector and V is the vector of residuals. GPS satellite clock offsets and orbits come from IGS post products. The detail model about PPP can be found in the following references such as Zumberge et al (1997), Kouba and Herous(2001), etc. This report will not focus on the details of PPP as many literatures can be referred.

2.3 Precise point positioning implementation and instructions

A post-processing software, named "TriP" (Precise Point Positioning—3P), has been developed by the author, from School of Geodesy and Geomatics, Wuhan University of China. "TriP" software, written in standard C, uses recursive least squared (RLS) as the estimator in pure absolute positioning mode and TriP is based on merely zero-differenced observation. Figure 2.3 gives a brief flow chart of the algorithm. Presently, it runs in DOS prompt mode, it has the possibility to do batch processing for large campaigns. It also will be updated to window-interface-based running mode soon. The processing procedure is very simple. You need only to download the proper precise orbit and clock files from IGS analysis center, and edit a very simple input control file, specifying the following information: the session beginning time and ending time, processing in kinematic or static mode, estimate the zpd or not, correct the earth tides correction or not (Airplane in the air has no earth tides influence), and antenna height (to phase center), rinex files name (*o file and *n file) and precise orbit and clock file names (in SP3 format) as well. Furthermore, two advance options

are available to professional user using these options, the user can tune the cycle slip detection threshold according to the data quality and have the chance to mask the satellite with bad quality observation.
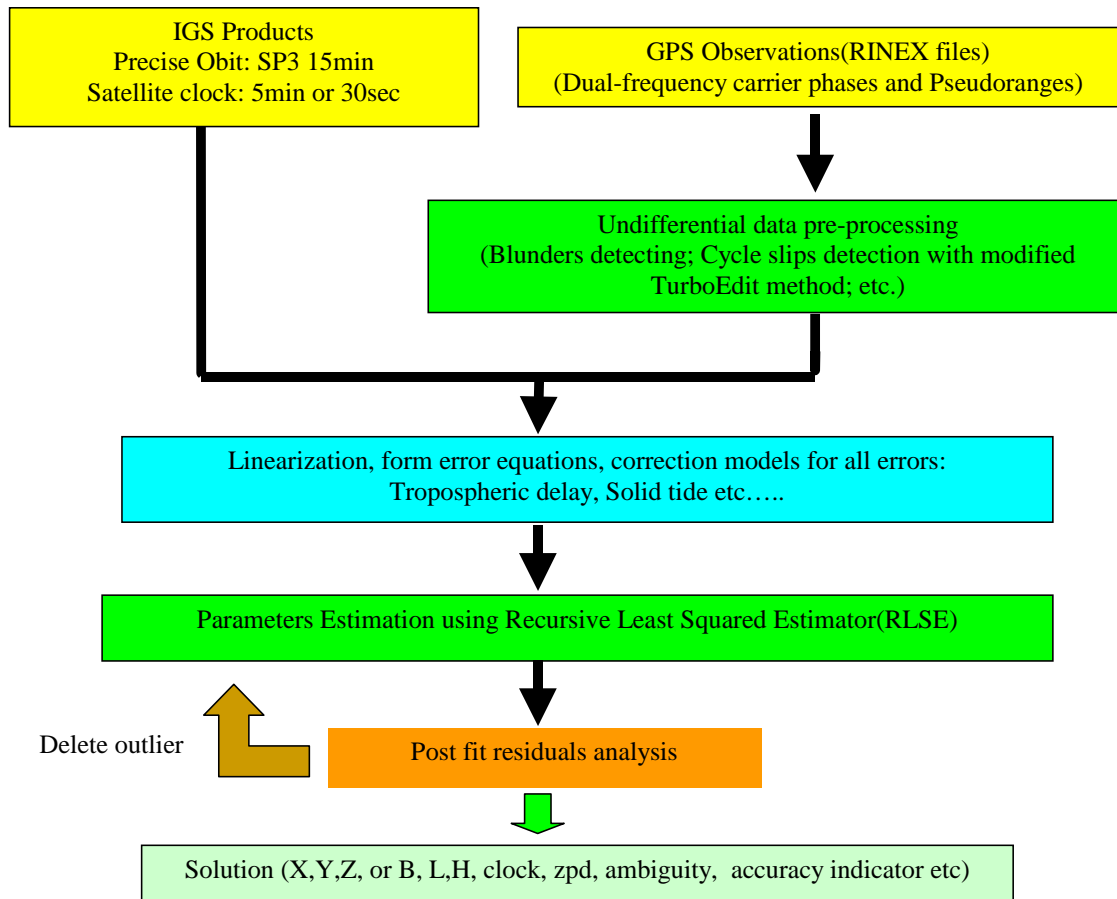
Fig 2.3 Flow chart of the algorithm

Sample input file for the TriP software (named as TriP.inp):

```
Session_beginning_time   = 0
Session_ending_time      = 24
Static_or_Kinematic      = 1      ( 0:static; 1: kinematic   )
Estimate_zpd_or_not      = 1      ( 0:NO;    1: YES          )
Observal_interval        = 1      ( interval of the observation )
Antenna_Height_to_APC    = 0.00   ( To antenna phase center  )
Tides_Corretcion         = 0      ( 0:NO;    1: YES )
Delete_Worst_Satellite   = 999    ( PRN: 1,2,...31, 999 default)
Rinex_obs_file_name      = air3131w.05O
Rinex_nav_file_name      = air3131w.05n
How_many_days            = 2      ( 1:one day,  2:obs file cross over midnight)
IGS_SP3_file_name_1      = cod13223.eph
IGS_clk_file_name_1      = cod13223.clk
IGS_SP3_file_name_2      = cod13224.eph
```

IGS_clk_file_name_2   = cod13224.clk

The output files include:

diagnose.txt: diagnose the stop epoch if program stops abnormally.

satamb.info: contains the satellite initial ambiguities, indicates the frequency of occurring cycle slips.

trip.kin or trip.static: position for kinematic solution in format of : GPS time(week second), latitude(decimal degree), longitude(decimal degree), ellipsoid height(meter), RMS, X, Y, Z, Hour, min, second, decimal hours;
and static solution in format of : GPS time(week second), X, Y, Z, latitude(decimal degree), longitude(decimal degree), ellipsoid height(meter), unmodelled zpd, RMS;

trip.res: contains epoch time line and satellite list, satellite PRN number, unweighted residuals of ionosphere free combination observation, satellite elevation angle (degree), initial ambiguity and fix ambiguities of ionosphere free combination phase observation.

plot.res: unweighted residuals of ionosphere free combination observation epoch by epoch in continuous list for each free cycle slip arc.

rms.rpt: weighted and unweighted RMS of solution. Generally, the smaller the RMS, the better the solution.

3 Evaluating TriP by making different comparisons

3.1 Airborne GPS data description

Kinematic GPS positioning is the key positioning method for the aircraft in airborne survey. GPS dual-frequency phase data were logged at 1Hz using 1~2 ground reference receivers at one or more reference sites, and 3~4 aircraft receivers (Trimble ssi, Ashtech UZ-12, and Javad type). The aircraft GPS receivers are named AIR1(Trimble, 4000-SSI), AIR2 (Ashtech, Z-extreme) and AIR3, AIR4(Javad, Legacy). AIR1, AIR3, AIR4 share the front GPS antenna; AIR2 uses the rear GPS antenna. Antenna offsets were unchanged from earlier KMS installations in OY-POF. Data were logged internally in receivers during flights, and downloaded upon landing on laptop computers. And all the data were converted to the RINEX format text file. In this report most GPS data come from Danish National Space Center and KMS airborne survey in Arctic and Greenland regions, including the GOCINA (2003), CRYOVEX (2004) and SPICE (2005) projects. The author participated in the SPICE2005 campaign flown from 2nd to 6th of August, 2005 from Kangerlussuaq in the western Greenland.

3.2 Comparison of processing time

GPS data processing time is always a concern to the end user. Especially for big campaigns, GPS data processing time is considerable due to the amount of flights. Table 3.1 provides an example of comparison of the processing time for a single kinematic solution made with GPSurvey 2.30 and TriP. The data session includes nearly 6 and half hours GPS data with 1 second interval is from 10: 3:15.00 to 16:40:53.00 on 2005-8-5. Both GPSurvey and TriP ran on the same laptop with Pentium 4 processor 1.8GHz. The processing time is counted from the data loading to processing finish. TriP processing speed is much faster than GPSurvey processing speed (about 10 times).

Tab. 3.1 Processing time with TriP and GPSurvey.

Software	Time consuming
GPSurvey	38min
TriP	2~3min

3.3 Static positioning and accuracy evaluation

TriP can process both static data and kinematic data. The software has two processors to meet the users options. In the SPICE 2005 campaign, there are two referenced stations (SFJ1 and SFJ2), the data on reference stations are collected with 1sec

interval. The repeatability for different days of TriP computed static solutions for the SFJ1 reference station is shown in table 3.2.

Tab. 3.2 Repeatability of TriP static solution

Point	DOY	X	Y	Z	Observation time
SFJ1	213	1582771.012	-1932979.301	5848888.560	8h
	214-a	1582770.977	-1932979.241	5848888.565	17h
	214-b	1582771.045	-1932979.208	5848888.560	4h
	215	1582770.972	-1932979.206	5848888.550	9h
	216	1582770.973	-1932979.201	5848888.543	9h
	217	1582770.935	-1932979.233	5848888.541	6h
	218	1582770.948	-1932979.230	5848888.541	16h
Averaged position		1582770.980	-1932979.231	5848888.551	
Standard deviation		0.035	0.032	0.009	
Known coordinate from Auto GIPSY		1582771.010	-1932979.208	5848888.526	
Difference between known and Averaged		0.030	0.023	0.025	

PPP solutions for the SFJ1 and SFJ2 stations are calculated using TriP, the difference between the two sets of coordinates generates the baseline vector, and this vector is compared to the vector optained using GPSurvey. The result is given in Table 3.3.

Tab.3.3 Baseline vector of SFJ1-SFJ2 comparison between GPSurvey and TriP on 215(DOY) in 2005.

Baseline	Dx	Dy	dz	Occupation Time	Solution Type	Baseline Slope Distance	Reference Variance	RMS	Variance Ratio
Sfj1-sfj2	-267.498	-648.023	-146.966	09:13:23.00	L1 fixed double difference	716.302	1.620	0.004	10.3
Sfj1-sfj2	-267.509	-648.030	-146.984	TriP solution on two reference station, and making difference derive the vector					
Diff	1.1cm	0.7cm	1.8cm	Difference between GPSurvey baseline vector and TriP vector					

Table 3.2 shows that the static positioning has good repeatability and also agree within a few centimeters with known coordinates from Auto GIPSY. It is normal for few hours GPS data when you use PPP to do positioning. (If you upload the same static GPS data to AUSPOS, SCOUT, CSRS, and Auto GIPSY, the final solution sometime has big differences). For PPP mode, the longer the observation, the higher accuracy you can have. One-day PPP solution can reach few mm level. In table 3.3 the short baseline from excellent double-differenced solution and TriP solution also agrees with each other very much.

3.4 Kinematic solution and accuracy evaluation by internal consistency validation

3.4.1 Static data simulate the kinematic solution epoch by epoch

An evaluation of the kinematic position accuracy achieved using TriP was made by comparing epoch by epoch of a forced kinematic TriP solution for a reference station to the known coordinates of that reference. The example data was taken from the GOCINA (2003) campaign on day 186. The reference station of SYY1 was used. Its known coordinates came from an Auto GIPSY solution. Figure 3.1 shows the unweighted residuals of the combined observations. Figure 3.2 gives the RMS from TriP kinematic solution on a static base station epoch by epoch. Figure 3.3 shows the difference between the TriP solution and known coordinates in NEU epoch by epoch.
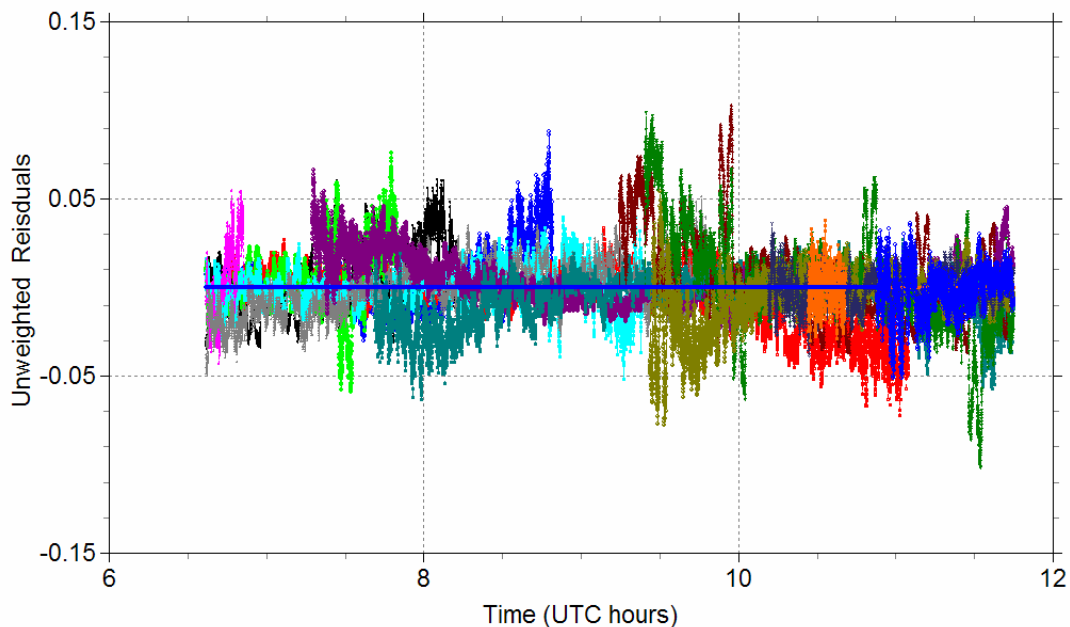
Fig 3.1 Unweighted observation (ionosphere-free carrier phase combination) residuals of all valid satellites from TriP kinematic solution epoch by epoch by using static GPS data of site SYY1 on 186 DOY, 2003.
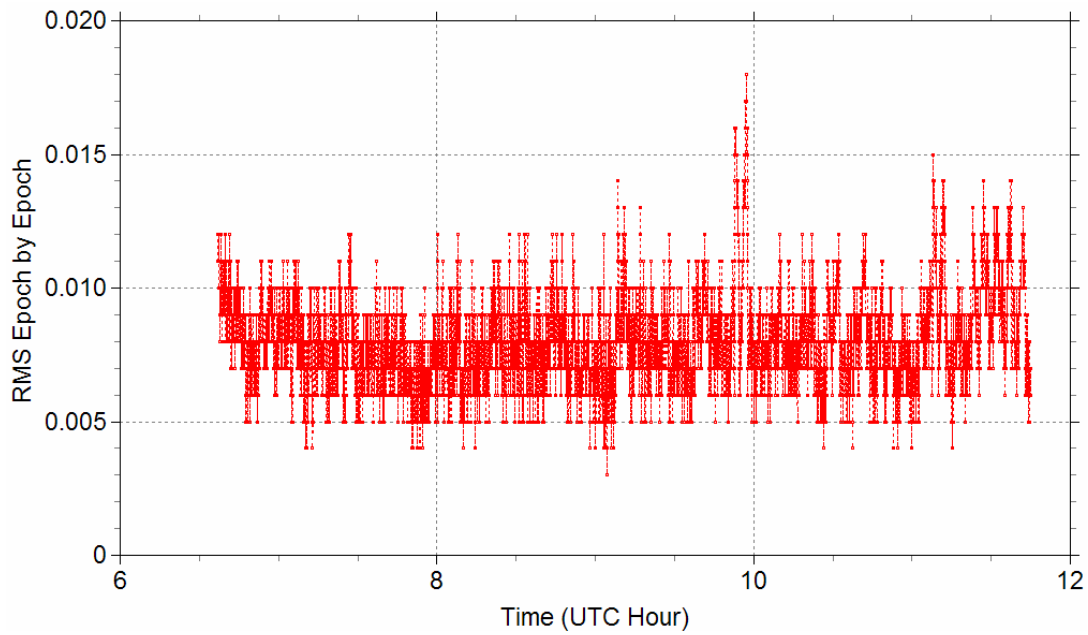
Fig. 3.2 RMS from TriP kinematic solution on a static base station epoch by epoch (site SYY1 on 186 DOY, 2003).
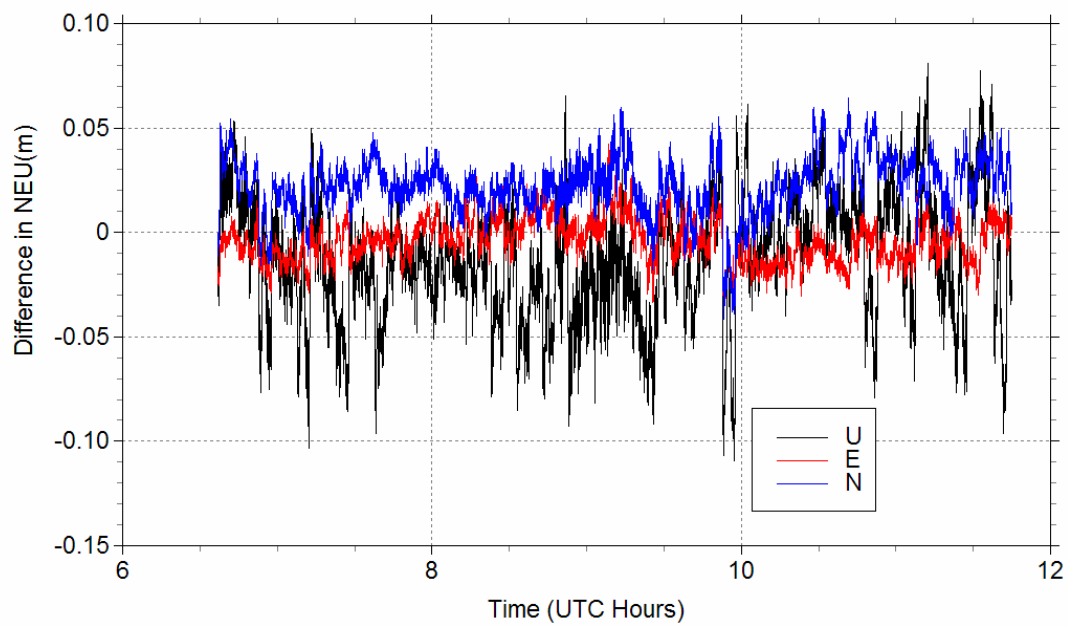
Fig 3.3 Compare TriP kinematic solution with known coordinates epoch by epoch (NEU) by using static GPS data of site SYY1 on 186 DOY, 2003.

Tab. 3.4 statistic result of above simulation comparison using static data from Fig3.3

Vector	N	E	U
Bias	-0.022	-0.004	-0.013
Standard deviation	0.014	0.010	0.029
RMS	0.026	0.011	0.032
Max.	0.064	0.042	0.081
Min.	-0.042	-0.033	-0.109

The simulation indicates impressive accuracy of the TriP kinematic solution could be achieved, 3D RMS are better than 5 cm. Generally, static GPS data quality is better than airborne GPS kinematic data, so static data simulate kinematic solution makes the accuracy look better than real kinematic positioning (see the following sections).

3.4.2 Comparisons of trajectories between two receivers sharing one antenna

The aircraft GPS receivers AIR1, AIR3, AIR4 share the front GPS antenna, if there is no observation error and model errors, using the GPS data of AIR1, AIR3 and AIR4 should produce the same trajectory as they share the same antenna. Thus, the differences between them reflect the kinematic positioning accuracy and ability to some extent. Figure 3.4 and table 3.5 shows the differences from an example flight. The 3D RMS also is quite good. The differences mainly came from the observation noise of different GPS receiver. Different receivers have different data quality, with different cycle slip happening and multipath. (AIR1 uses Trimble, AIR2 use Javad)
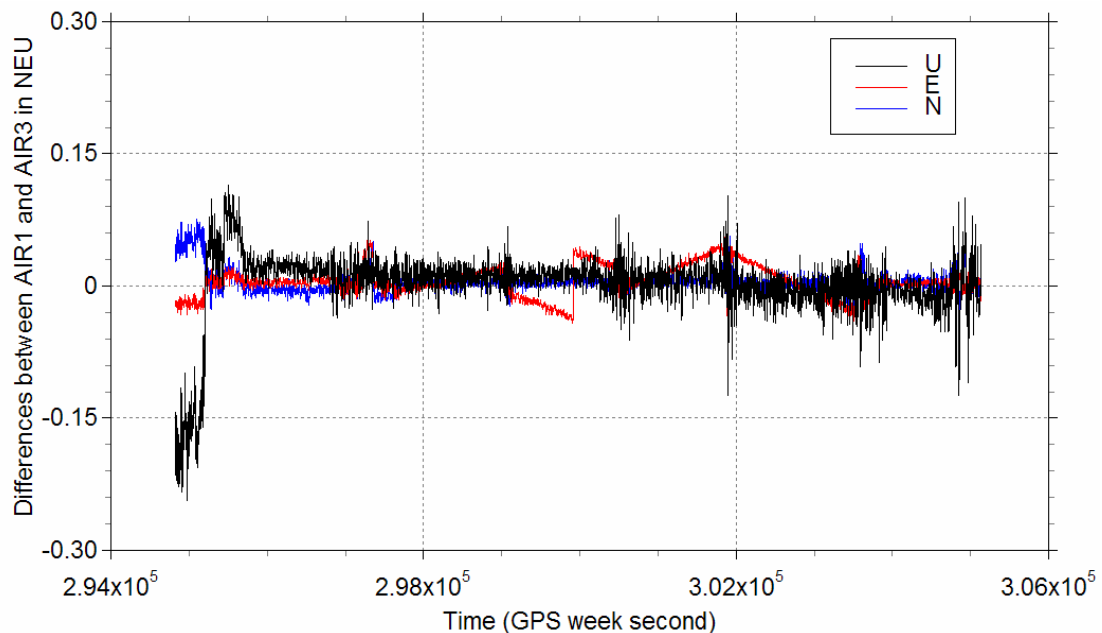

Fig.3.4 Differences of AIR1 and AIR3 from the same flight (DOY 215 in SPICE 2005)

Tab. 3.5 Statistic comparison of the difference of AIR1 and AIR3

Vector	N	E	U
Bias	0.005	0.005	0.002
Standard deviation	0.013	0.017	0.039
RMS	0.014	0.018	0.039

3.5 Comparisons between TriP and other GPS software with ground truth

3.5.1 GPS data sets

In the previous section, the comparison shows optimistic result of TriP kinematic solution by using internal consistency checking. The following sections will focus on the comparison between TriP solutions and other software solutions and also with ground truth. GPS data from two long-range flights were used to do the comparison.

The first flight of airborne survey was conducted on July 5, 2003 in the Arctic supported by the Geoid and Ocean Circulation in the North Atlantic (GOCINA) project (Figure 3.5). The airborne measurements were done with Air Greenland's Twin-Otter OY-POF. The aircraft took off at 12:46(UTC) and landed at 16:29 giving a total of 3 hours and 42 minutes of flight time. The flight started from Stornoway, Hebrides and ended at Hornafjordur, Iceland. Since the first flight was over open sea, the sea topography and the altimeter measurements was used as ground truth data.
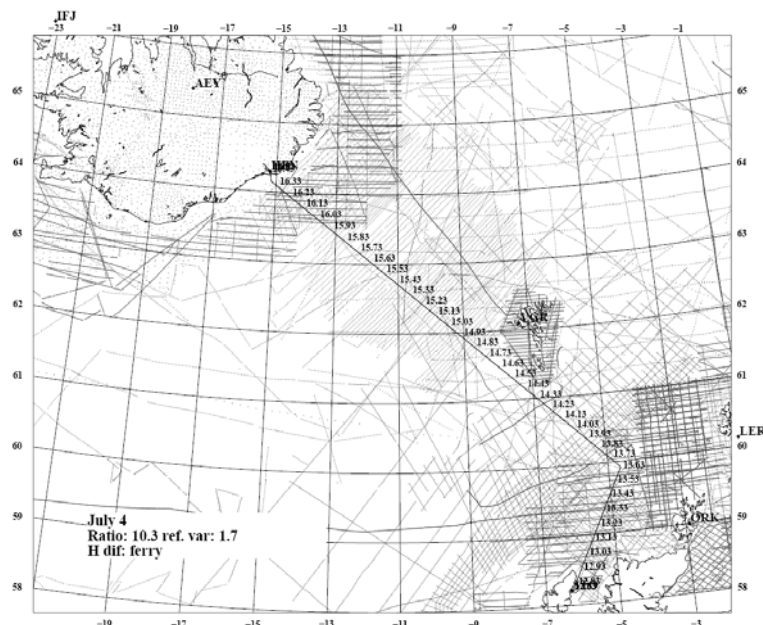
Fig.3.5 Flight trajectory on JD 186 (July 5, 2003)

The second flight, showed in Figure 3.6, on JD 146 (May 25, 2004) was part of the GreenICE/SITHOS flights performed by the Danish National Survey and Cadastre in the spring of 2004. The flight time was 6 hours, starting at Alert, Canada at 16:46 UTC and returning to Alert at 22:46 UTC.

The flight path was planned to follow the track of ICESAT towards Northeast, North of Greenland. The second flight on JD 146 partially was designed to overlap the ICESat along track profile in the same day, and the ICESat footprint was used as ground truth. Figure 3.6 shows the second flight profile overlap partially with ICESat footprint track. The thin line in Figure 3.6 is the flight trajectory, the bold line with are ICESat footprint tracks on the same day of May 25, 2004. There are two parts of the trajectory overlap the ICESat footprint's ground track. We identify them as track I (right in Figure 3.6) and Track II(left side in Figure3.6) in this report.
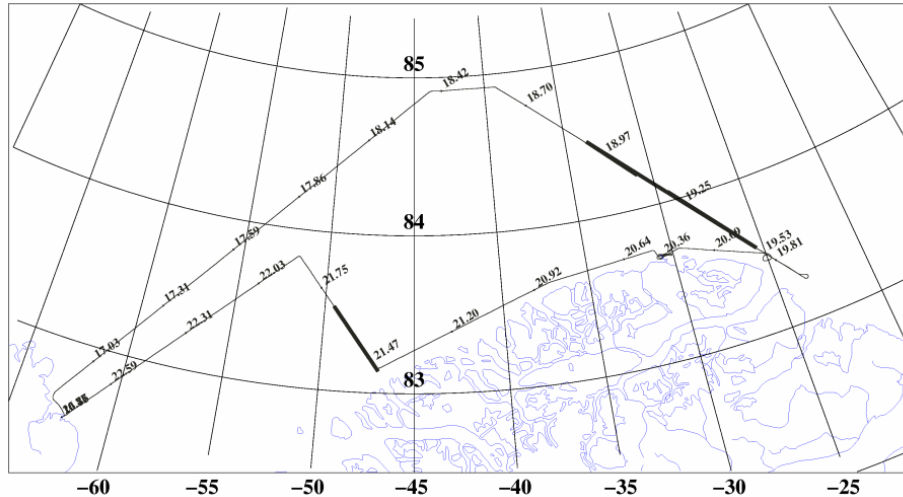
Fig.3.6 Flight trajectory overlaps the ICESat footprints profile partially on May 25, 2004

Reference receiver coordinates for both flights were computed using Auto GIPSY of JPL and typically have accuracy better than 5 cm, which will be used by double difference software. IGS precise orbit and clock files were downloaded from IGS center (http://igscb.jpl.nasa.gov/igscb/product/).

3.5.2 Comparisons between trajectories from different GPS softwares

Four different GPS software systems have been used to process the kinematic GPS data, they are GPSurvey, GrafNav/GrafNet 7.50, "IT" and "TriP". GPSurvey, Timble's post-processing software, has been widely used in the geodesy community for a long time. GrafNav/GrafNet is a Windows software package developed by Waypoint Consulting Inc, Canada. The "IT" ("Interferometic Translocation") software has been developed by Dr. Colombo from GEST/NASA, using Kalman filter and smoother as estimator in both relative and absolute positioning mode. "TriP" (Precise Point Positioning—3P) software was developed by the author. The "TriP" software, written in standard C, used recursive least squared (RLS) as the estimator in pure absolute positioning mode.

Using the GPSurvey solution as a reference, differences between solutions from each software were made. The NEU differences between the GPSurvey trajectories and each of the other software trajectories are shown in the following figures. Figure 3.7 shows the 186 flight (2003) trajectory differences. Figure 3.8 gives the 146 flight (2004) trajectory differences. There are two reference stations available for both flights, and only GrafNav has the option to process the baseline using multiple base stations data at the same time, and the combination solution will be generated by GrafNav automatically if preferred. GPSurvey always use one reference station to derive the whole trajectory, while IT and TriP process the GPS data without base station but using IGS products. Comparing (a), (b), (c) in Figure 3.7, it seems that the PPP solution is a little bit noisier than the double difference solutions, which mainly comes from the interpolation of the satellite clock as the IGS clock interval is 5min or 30 sec. Even SA is off, but the clock behavior cannot be simply interpolated with a simple mathematical model. It will be improved if the 30 sec clock offset is available. In figure 3.7, the big discrepancy between GrafNav and GPSurvey at the end of the

survey after the plane landed, because the receiver on the near end was turned off, so GrafNav only used the far end base station data, the solution degrade down sharply. And also for the second flight, in figure 3.8, the GrafNav solution in the middle has bigger differences than the beginning and ending stage as the aircraft is far away from the base station. This does not occure in the PPP solutions in (b) and (c) of figure 3.8. IT uses Kalman filtering but TriP uses recursive least squared, so the solution is different as seen in (b) and (c) in Figure 3.7 and Figure 3.8. Some spikes from the IT solution is seen.
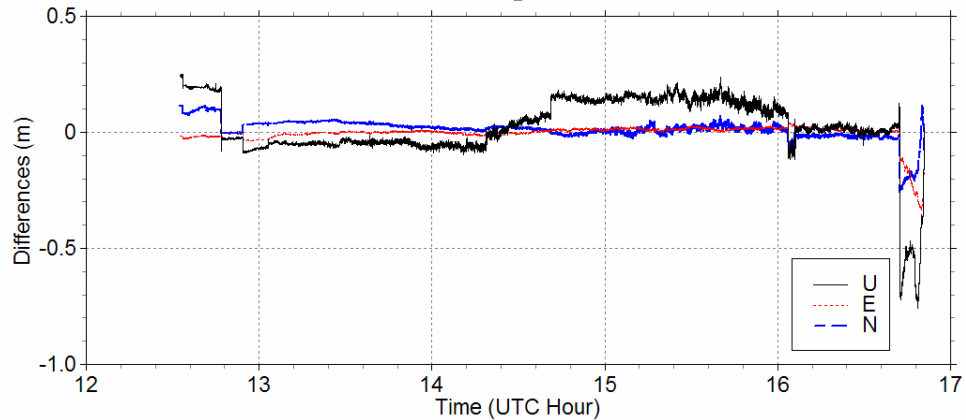
(a). Differences between Waypiont and GPSurvey solutions epoch by epoch
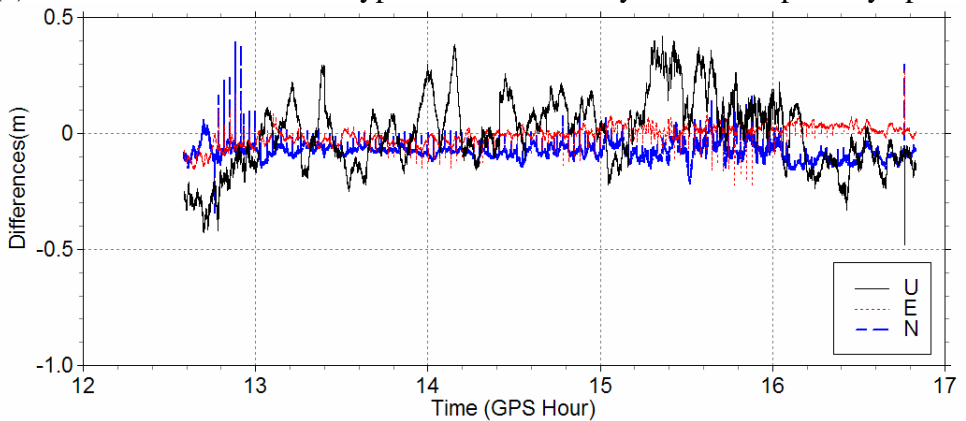
(b). Differences between IT and GPSurvey solutions epoch by epoch
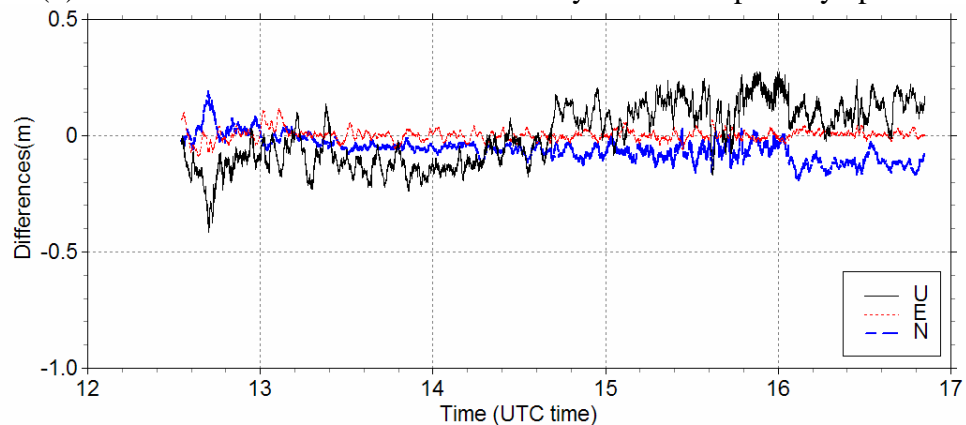

(c). Differences between TriP and GPSurvey solutions epoch by epoch

Fig. 3.7 Differences between solutions from different GPS software of DOY 186 flight, 2003.
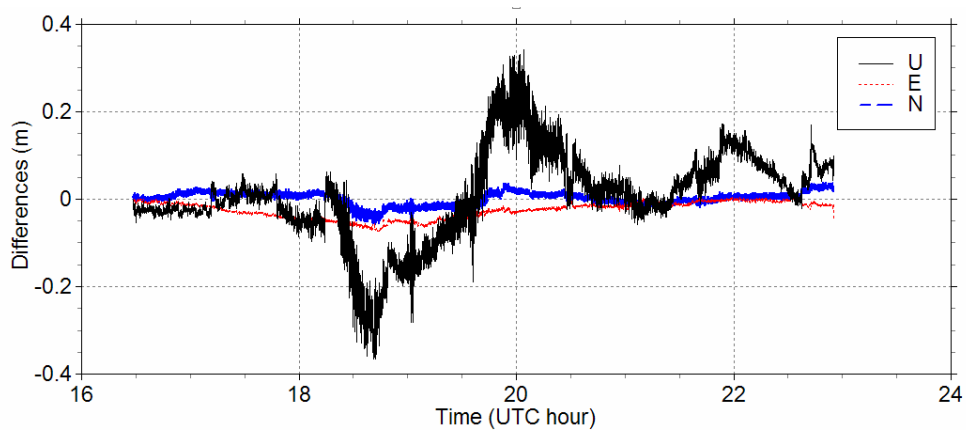
(a) Differences between GrafNav solution and GPSurvey solution epoch by epoch
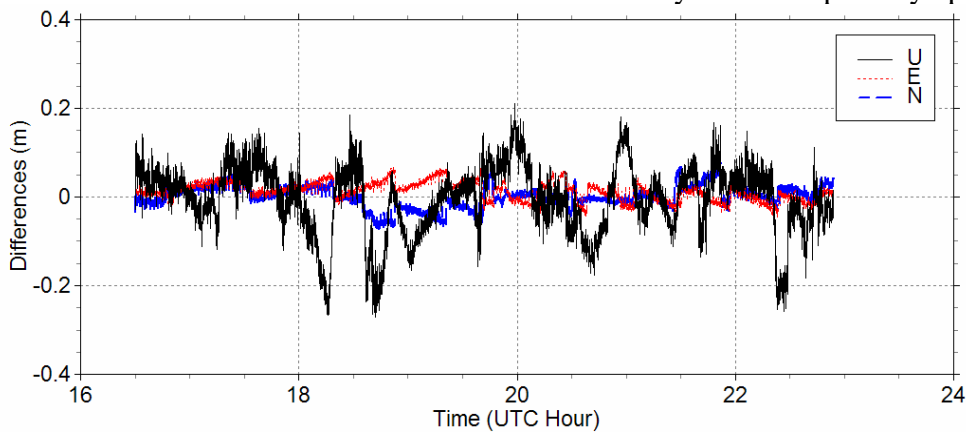
(b). Differences between IT (PPP mode) and GPSurvey solutions epoch by epoch
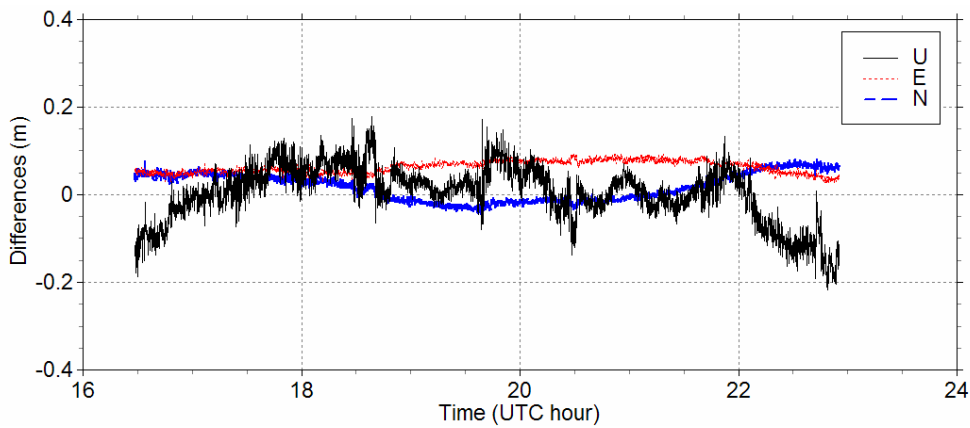
(c). Trajectory differences between TriP solution and GPSurvey solution by epoch

Fig. 3.8 Differences between solutions from different GPS software of DOY 146 flight, 2004.

3.5.3 Comparison with SSH

For the flight of DOY 186 in 2003, we compare the flight height using the laser altimeter and sea surface height. The results are shown in Table 3.6, Figure 3.9 and Figure 3.10. The low pass filter was used to smooth the wave noise which has influence on the laser altimeter. Figure 3.9 and Figure 3.10 shows the differences between laser altimetry height of sea surface and sea surface height before and after filtering.
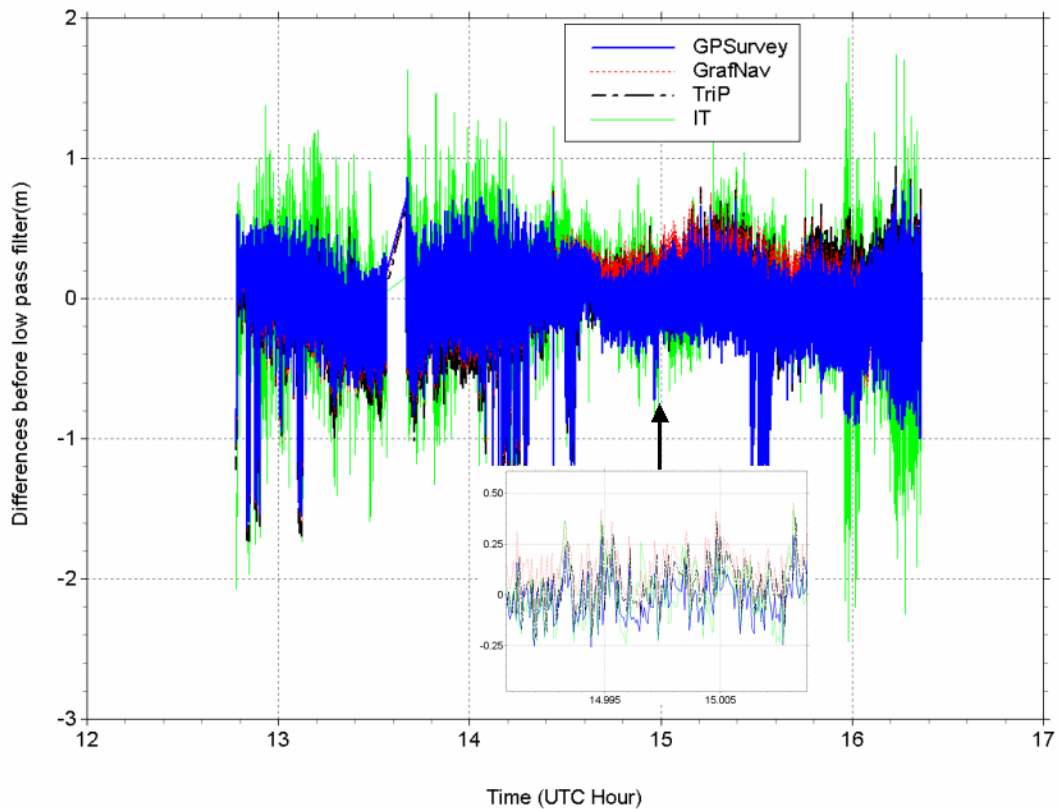
Fig 3.9 Differences between the airborne laser altimetry sea surface height and true sea surface height before low pass filtering
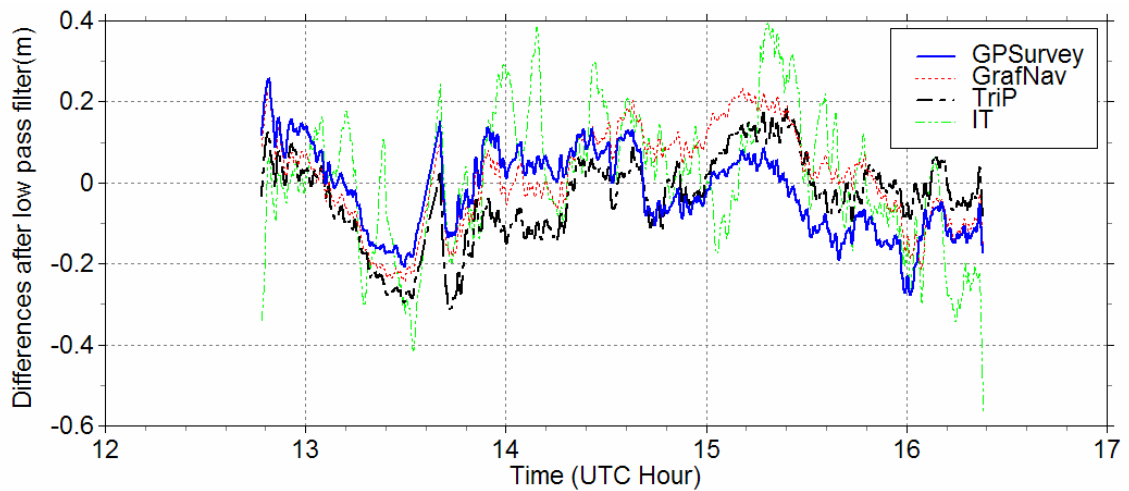

Fig 3.10 Differences between the airborne laser altimetry sea surface height and true sea surface height after low pass filtering

Tab.3.6 Statistic differencing between 4 software solutions of flight on DOY186 with respect to "ground truth" (Sea surface height)

Soft.	GPSurvey	GrafNav	TriP	IT
Mean	-0.02	0.02	-0.03	0.01
Std.	0.10	0.12	0.11	0.17
RMS	0.10	0.12	0.11	0.17

The solutions mean biases are slightly different from each other, but their RMS nearly are at the same level, the IT RMS is slightly bigger than the other three solutions. The airborne laser altimeter measurements of sea surface height much agrees with the sea surface height derived from dynamic ocean topography, accurate tide model and geoid on cm level. Figure 3.10 and Table.3.6 demonstrate the long range kinematic positioning ability can reach 1~2 dm in the vertical.

3.5.4 Comparison with ICESat

For the second flight, the ICESat footprint height was used as ground truth. The predicted accuracy of ICESat/GLAS geolocated products for the surface elevation measurements is 15 cm, averaged over 60 m diameter laser footprints spaced at 172 m along track (Zwally etc., 2002). As the sea ice is flat, apart from small roughness, although the size of ICESat footprint is much larger than the airborne lidar footprint size, we can consider that the footprint height represent the averaged height of the footprint area. Examples of the statistic differencing between height of airborne lidar footprints with different GPS solutions and the "ground truth" height of ICESat footprints are summarized in Table 3.7. The result shows their standard deviation is on the same level as comparison with SSH.

Of course, GPS positioning error, lidar range error, orientation error, lidar pointing error, etc also contributes to the differences. And also, the "ground truth" from ICESat data is contaminated by errors. The roughness of the surface also makes them different, because the ICESat footprint size is 60 m, while the airborne lidar footprint size is only about one meter, but such noise could be smoothed by GEOGRID. However in above error sources, GPS positioning error dominates them. The differences between height of airborne lidar footprints and the "ground truth" height of ICESat footprints represent the performance of kinematic software systems.

Anyway, the heights from the above software systems have much agreement between each other, only a bias of 1~2 dm is seen between the height of airborne lidar point and ICEsat footprint. The bias possibly comes from both ICESat data and airborne data.

Comparing Table 3.6 and Table 3.7, it is seen that coincidence between airborne lidar and ICESat is not as good as it is between airborne altimeter and sea surface height. For precise point positioning, bias could be coming from the IGS products, since you have few hours data, and during this time, the orbit or clock possibly is away from the true value, and in PPP we always fix the orbit and clock as the known input reference.
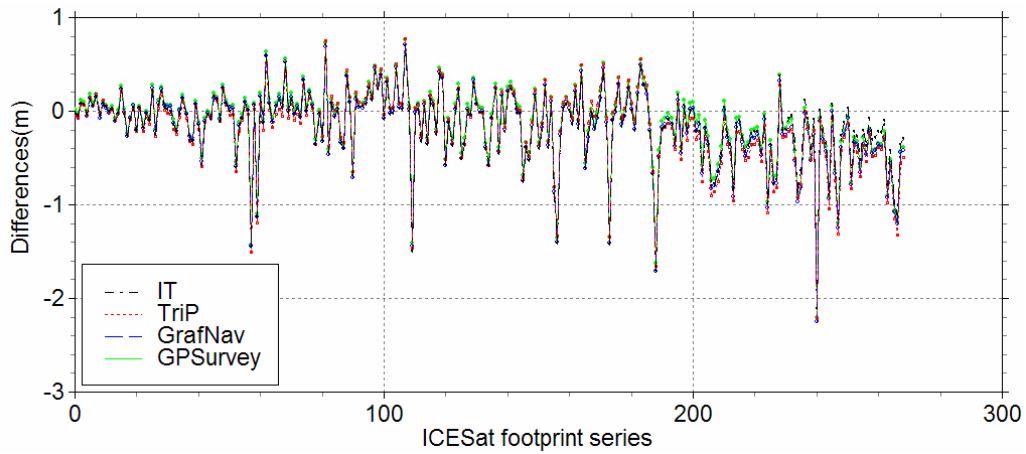
Fig 3.11. Differences between the airborne laser altimetry and ICESat footprints

Tab.3.7 Statistic differencing between 4 software solutions and ground truth from ICESat

Track	I				II			
Selected points	57				269			
Software	GPSurvey	GrafNav	IT	TriP	GPSurvey	GrafNav	IT	TriP-I
Mean	-0.19	-0.13	-0.19	-0.18	-0.12	-0.16	-0.15	-0.17
Std. Dev.	0.29	0.30	0.29	0.30	0.40	0.40	0.38	0.41
Min.	-1.00	-0.95	-0.99	-0.99	-2.20	-2.25	-2.11	-2.21
Max.	0.31	0.36	0.31	0.27	0.76	0.71	0.71	0.77

4 Examples of TriP applications

As discussed in the previous chapters, TriP solutions for the kinematic case could reach cm to dm level. Almost all kinematic GPS surveys can use TriP to recover the trajectory epoch by epoch by using IGS products. In this section, three examples is demonstrated.

4.1 Airborne Survey

The GPS solutions for the aircraft antennas in airborne survey were done on basis of IGS final orbit and clock products using TriP software. Generally all the GPS receiver data were processed, and the trajectories between AIR1, AIR3 and AIR4 (they share the same antenna) were compared with a simple program named "diffneu.exe". Based on the differences between each other, a "best" solution can be selected as the basic GPS aircraft solution. These solutions are generally estimated to be accurate to below the 20 cm RMS level (as discussed previously). The turbulence of the aircraft, the valid visible satellite number and GDOP, and IGS products quality may mainly influence the solution accuracy. Most of flights GPS data quality is OK.

An example is shown in Figure 4.1. There was an interval of static observation before take off and after landing. Therefore, in figure 4.1, the plot at the beginning and ending keeps horizontal.
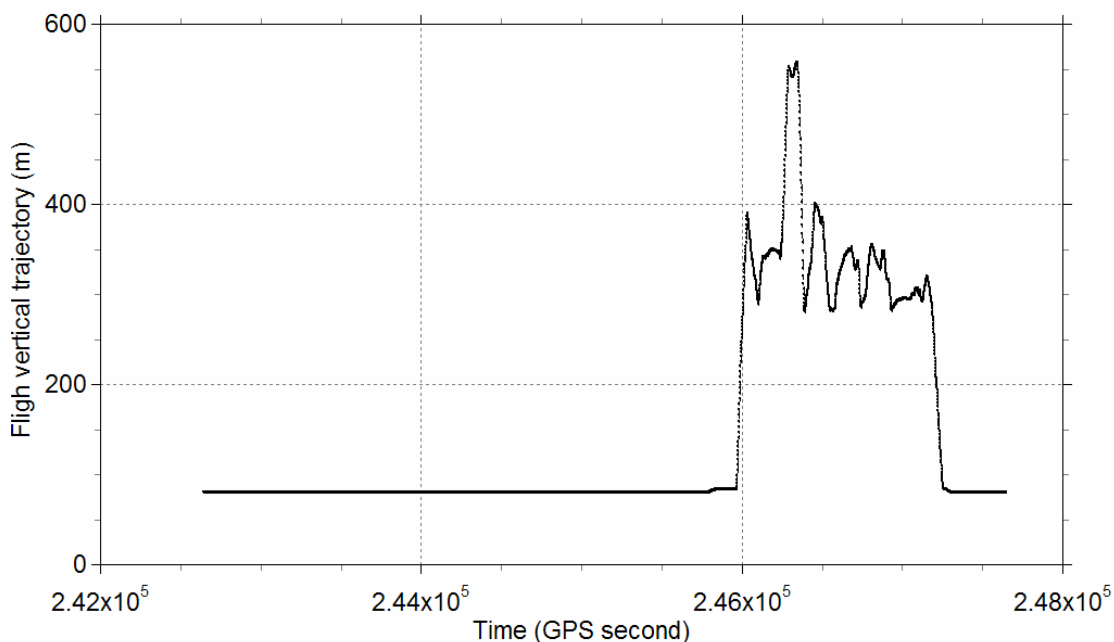

Fig 4.1 Height profile of test flight
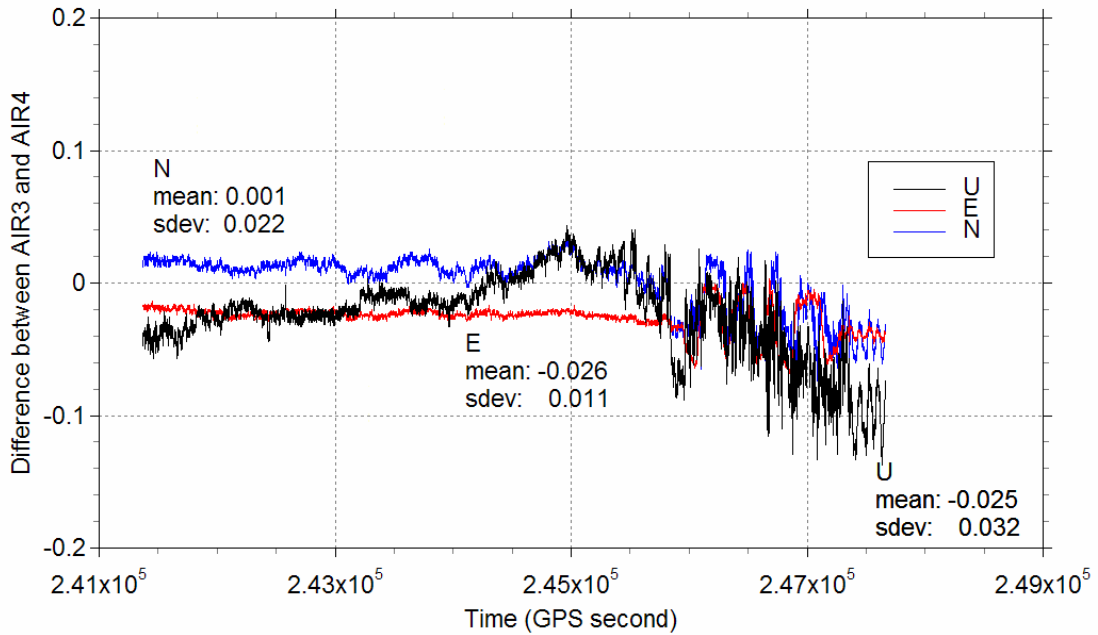
Fig 4.2 Trajectories difference between AIR3 and AIR4 (sharing one antenna)

Figure 4.2 is an example of the trajectory differences between two receivers that share the same antenna. The mean bias and standard deviation of NEU in figure 4.2 shows that the standard deviation of 3D position is only few cm. Figure 4.3 is the flight trajectory over an area of special interest.
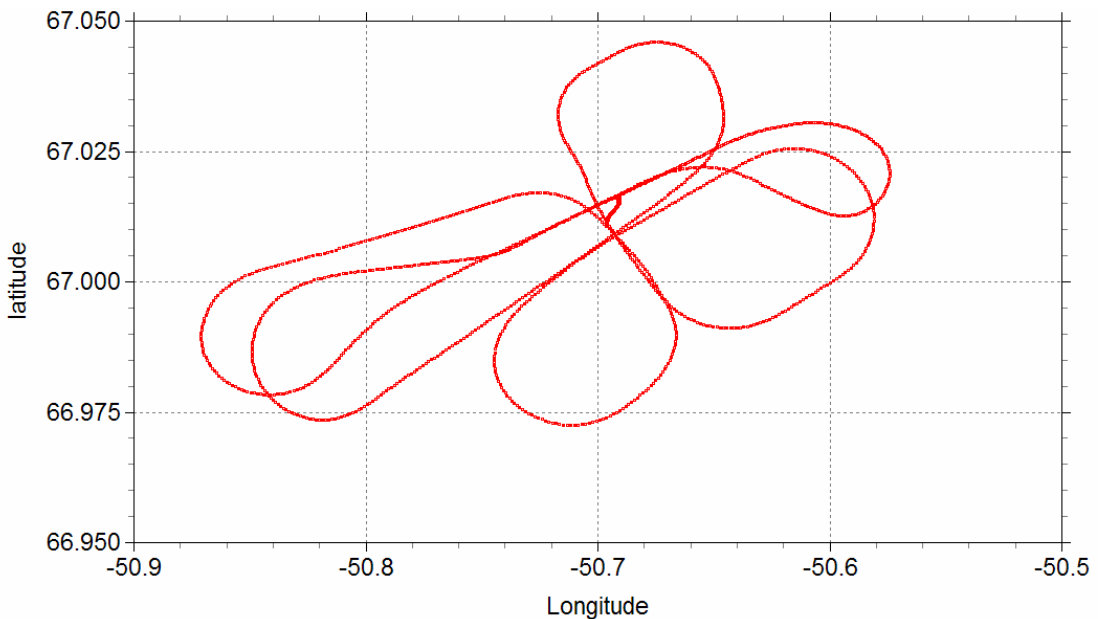

Fig 4.3 Trajectory of test flight (Four pass over a square building)

4.2 Retrieve the ocean tide from the GPS observation on Ice shelf

The GPS data set of this example came from Amery Ice Shelf, in Antarctic. Five continuous days of GPS observations were collected at the frontal part of Amery ice shelf by the author. The observation was started on 22, Dec. of 2003, ended on 27, Dec. of 2003. The Leica 530 dual-frequency GPS receiver was used. The interval was set to 10 seconds. GPS antenna was set on a tripod outside the tent nearby. The

geographic coordinates is Lat.: 69º26.27´S; Lon.: 71º26.18´E. In order to keep the cold air away from the receiver, the receiver was put in the tent. Three storage batteries were used to power the GPS receiver in turns. Leica530 GPS receiver has two power connectors, so the battery can be shifted manually without interrupting the observation. On Amery ice shelf, surface snow melts under the sun shining during daytime in the summer season. The tripod used for setting GPS antenna sank few decimeters per day. In order to keep the tripod stable during the observation, measures should be taken. Before setting up the tripod, three stakes were intruded into the ice surface under the three legs of the tripod to support the tripod legs. The GPS antenna was set on the tripod beforehand and kept it for few hours to make the tripod stable. Such procedure can basically ensure the tripod to be stable in the five days observing.

The surface height of an ice shelf varies in time with ocean tides, atmospheric pressure, ocean and ice density, snow loading, firn compaction, ablation or accretion of ice at the ocean/ice interface and ice dynamics. These processes act over a wide variety of time scales: from hours to decades or longer. The main cause of short-time scale height variability will generally be ocean tides. Although we can calculate the ocean tide from the ocean tide models, the current disadvantages are a lack of data in the Antarctic region. For example, most models rely heavily on assimilated TOPEX/POSEIDON which has a southern limit of 66°S, well to the north of all but a few of Antarctic's ice shelves. Consequently, the accuracy of the models often rest on spatially sparse tide gauge measurements. GPS is currently the most convenient and precise method available for the measurement of sub ice shelf tidal signals on a point-by-point basis. Using TriP to proces the continuous GPS data, the semidiurnal tide and diurnal tide signal can be found in figure 2. The figure shows that the difference between highest tide and lowest tide is about 2 meters, which coincide with the result of King's [3]. And also embed short tide signal. If the longer GPS data can be achieved, the more detail analysis can be made. And also, the GPS positioning result can be used to study the ocean tide around the Antarctic. On the other hand, to accurately monitor long-term trends in ice shelf surface height, the tide component must be removed from the height measurement, such that all ice shelf heights are referred to a"tide-free"datum.
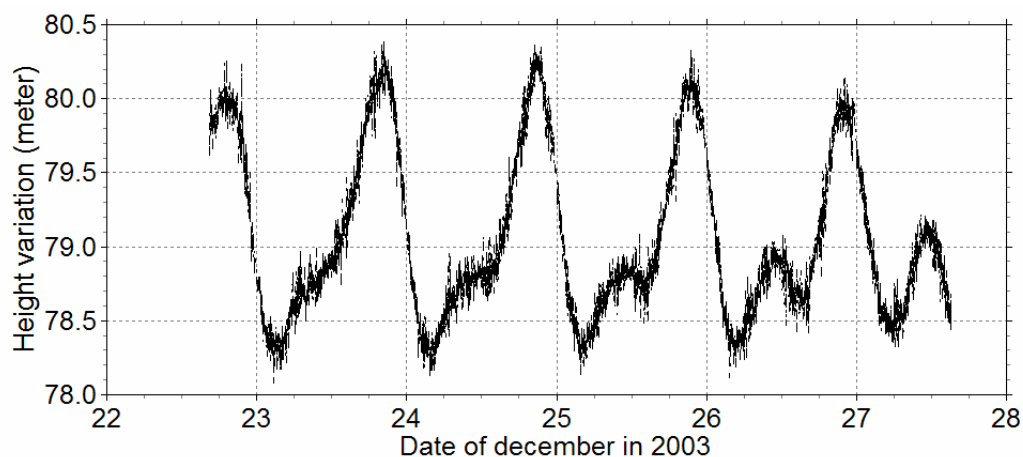

Fig 4.4 Height variation of the point in the frontal part of Amery ice shelf

4.3 Boat-borne GPS experiment for ocean topography and tide

The GPS antenna was mounted on the front part of a boat (Figure 4.5), The interval of GPS data was set to 1 sec. A Javad GPS receiver was used. The height from the antenna to the sea surface was measured in the cases of both stop and sailing. The Fjord of NUUK in west Greenland is narrow and long, the sea surface is quite calm, so only ocean tide and ocean topography will change the antenna height if the boat was kept at the same speed when sailed.

Fig. 4.5 Boat-borne GPS kinematic experiment in a Fjord of NUUK in Greenland
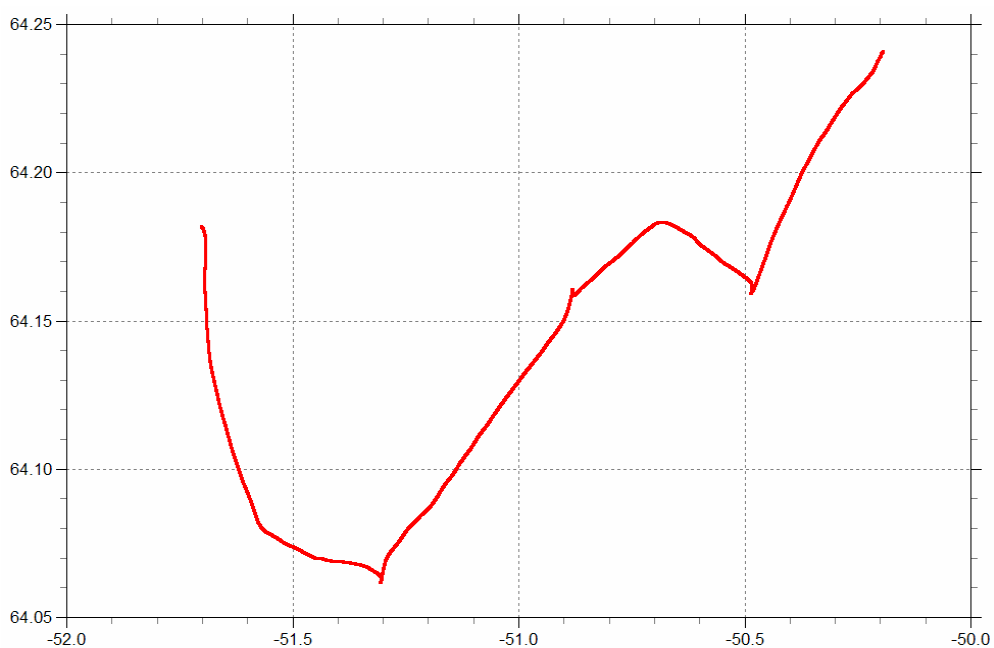
Fig. 4.6 Boat sailing trajectory in the Fjord
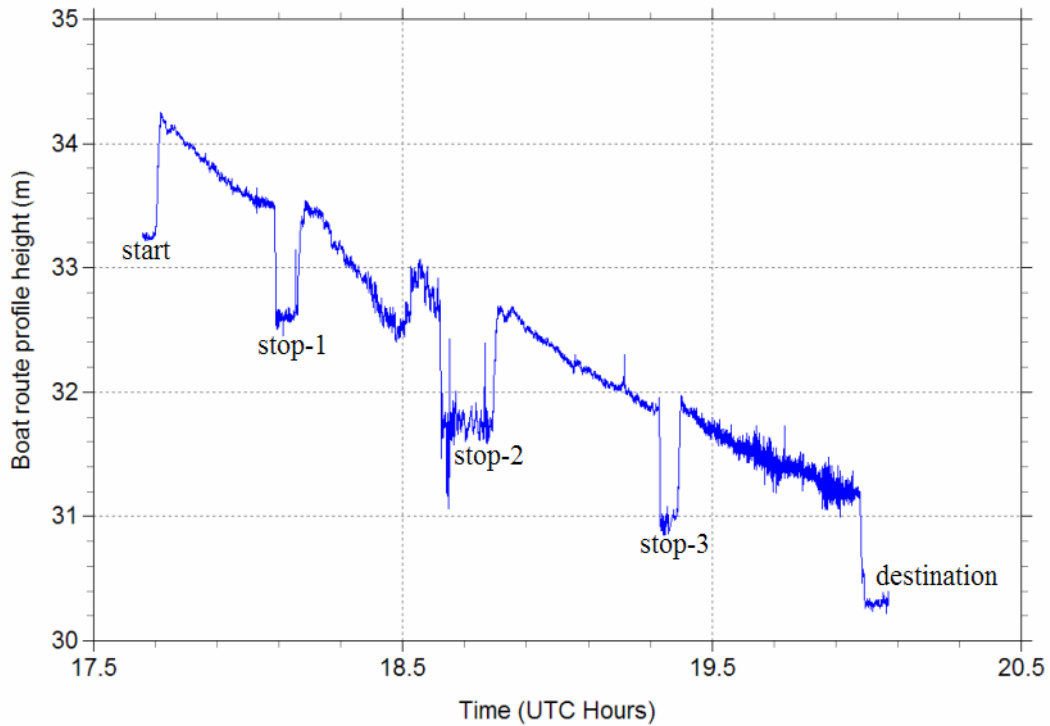
Fig. 4.7 Antenna height variation along the boat trajectory
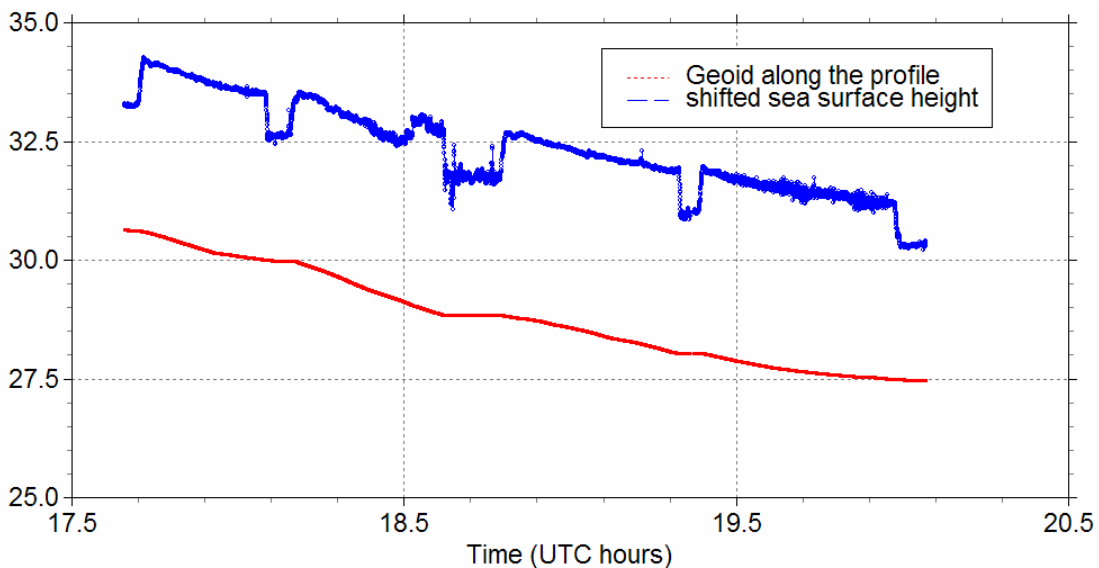
Fig. 4.8 Comparison between the sea surface height and geoid height along the boat trajectory

The slope of the boat height profile in figure 4.7 is mainly from the local geoid slope (see figure 4.8). At the start point, when the boat did not sail, the fore tip of the boat did not tilt up, once the boat where sailing, the fore tip of the boat tilted up. During the sailing, the boat was stopped three times to retrieve GPS receivers on land, so there was three drops of the height profile. And also we measured the height from the antenna to the sea surface at sailing and stop. The height differences coincides with such drop in the profile. However, before the second stop disturbance happened, possibly caused by ocean wave or geoid. It should be pointed out that the Fjord is considerable calm as the surface of a lake. Figure 4.9 is the absolute velocity of the boat. It is obvious that the boat was sailing at almost the same speed all the time.
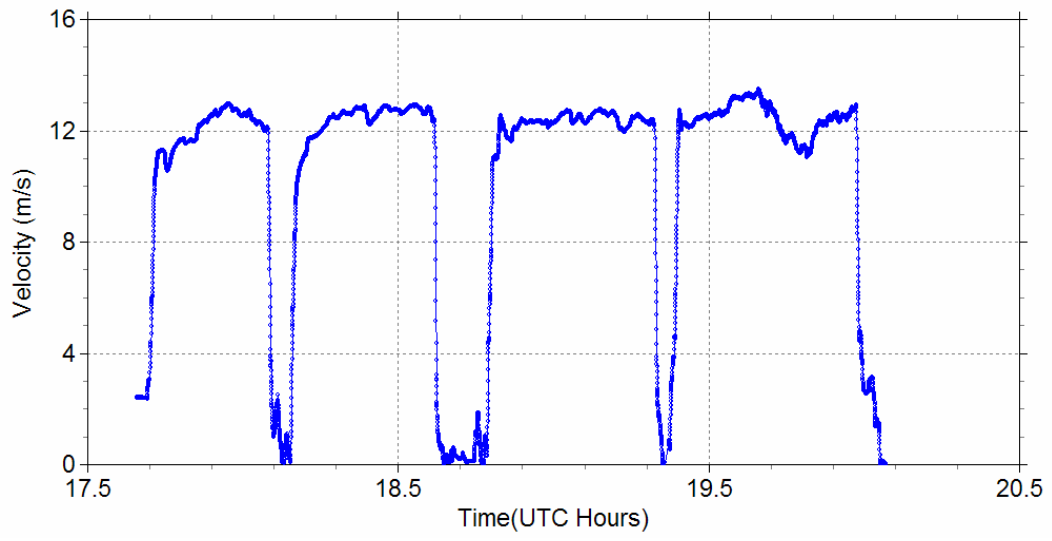
Fig. 4.9 Velocity of the boat

5 Airborne laser scanning system calibration

5.1 Introduction

Airborne laser scanners are capable of measuring heights to accuracies of 5-10 cm and horizontal positions to decimeter accuracy, depending on the type of terrain. The data can thus be used for applications such as DEM and DTM generation, urban mapping and modelling, corridor mapping, coastal and wetland monitoring, flood and risk assessment and forestry management. However, to guarantee this level of data quality the measurements must be as close as possible to misalignment free. Misalignment errors can be avoided through careful calibration procedures. Baltsavias (1999) presents an overview of basic relations and error formulas concerning airborne laser scanning and a large number of publications report the existence of systematic errors. The solution for dealing with and eliminating the effect of systematic errors can be categorized into two groups. One approach is based on the introduction of a correction transformation of the laser points to minimize the difference between the corresponding LIDAR patches and ground truth. Kilian (1996) presents a method of transforming overlapping LIDAR strips to make them coincide with each other using control and tie points in a similar way to photogrammetric block adjustment. The other technique attempts to rigorously model the system to recover the systematic errors. Burman (2000) treats the discrepancies between overlapping strips as orientation errors, with special attention given to the alignment error between the INS and laser scanner. Filin (2001) presents a similar method for recovering the systematic errors with respect to the boresight misalignment problem. Krabil et al. (2000) give a detailed description of the calibration procedures used with the NASA Airborne Topographic Mapper (ATM) sensor to correct laser range measurement and the angular mounting biases of the sensor relative to the INS system. Thiel and Wehr (1999) have also described the calibration procedures used for removing angular offsets in the mounting of the ScaLARS sensor (Institute for Navigation, University of Stuttgart). The ScaLARS instrument uses the Palmer scanning pattern, which produces an elliptical scan pattern with redundant data that can be used for calibration. In fact, even where careful calibration of the instruments has been carried out and specific operational procedures are followed, some errors can still be present in the data. A method of reducing or eliminating these remaining errors, or errors that are present if calibration or operational procedures are not properly employed, uses redundant (overlapping) data and external information, combined with a mathematical model of the errors, to correct the measurements. This technique is a self-calibrating, least squares strip adjustment, similar to methods used in photogrammetric aerial triangulation. The success of the adjustment is directly dependent on the ability of the mathematical model to correctly represent the errors in the data. However, the above presented method always using gridding of the lidar points to regular data to match the overlap patch.

In this section, a stepwise geometric method to retrieve the misalignment angles of an airborne lidar system will be investigated in detail. The developed technique is based on the availability of LIDAR points on a known regular shaped object with ground truth available. The LIDAR strips should be flown in certain pattern over the features as discussed later. Focus will be on calibration of misalignment angles as the levelarm and ranging offsets are determined before data processing.

5.2 Stepwise Geometric Method Conception

5.2.1 Boresight misalignments between INS and laser scanner

In airborne LIDAR systems, the navigation sensors are separated, since the GPS antenna is installed on the top of the fuselage while the INS sensor is attached to the LIDAR system, which is down in the aircraft. The spatial relationship between the sensors should be known with high accuracy. In addition, maintaining a rigid connection between the sensors is also very important since modeling any changes in the sensor geometry in time would increase the complexity of the system model and may even add to the overall error. The INS frame is usually considered as the local reference system; thus the navigation solution is computed in this frame. The spatial relationship between the laser scanner and the INS is defined by the offset and rotation between the two systems. The critical component here is the rotation since the object distance amplifies the effect of an angular inaccuracy, while the effect of an inaccuracy in the offset does not depend on the flight height and the offset can be accurately determined before hand. The coordinates of a laser point are a function of the exterior orientation of the laser sensor and the laser range vector. The observation equation is:

$$P_{Local} = R_{Attitude} \cdot (R_{misalignemnt} \cdot R_{scanangle} \cdot r_{laserrange} + \Delta f_{levelarm}) + APC_{local} \qquad (5\text{-}1)$$

in which:

P_{Local} is 3D coordinates of a laser point in the local mapping frame;

$R_{Attitude}$ is the rotation matrix between the INS frame and mapping frame, measured by GPS and INS;

$R_{misalignma}$ is boresight matrix between the laser frame and INS frame;

$R_{scanangle}$ is the transformation matrix from laser range to laser frame with scan angle;

$r_{laserrange}$ is the laser range from fired point to target;

$\Delta f_{levelarm}$ is offset between laser fire point and GPS antenna phase center in body frame;

APC_{local} is the 3D coordinates of GPS Antenna Phase Center in the local mapping frame.

The above equation gives the general relationship between different parts of the airborne lidar system. It is a nonlinear system. The procedure to retrieve the misalignment angle is always complicated and annoying. However, the following sections show that all the misalignment angles have different influences on the coordinates of laser footprints. That means we can retrieve the angles offset based on a stepwise geometric method because misalignments in roll, pitch and heading have different influence characteristics on lidar point position.

5.2.2 Influence of roll misalignment on laser points

In rolling, pitching and heading misalignment, only rolling misalignment deflects the horizontal flat surface (see Figure 5.1), and it also shifts the object position along the scanning direction (vertical to the flight direction). In figure 5.1, red footprints demonstrate deflected horizontal surface by misalignment in the roll angle.
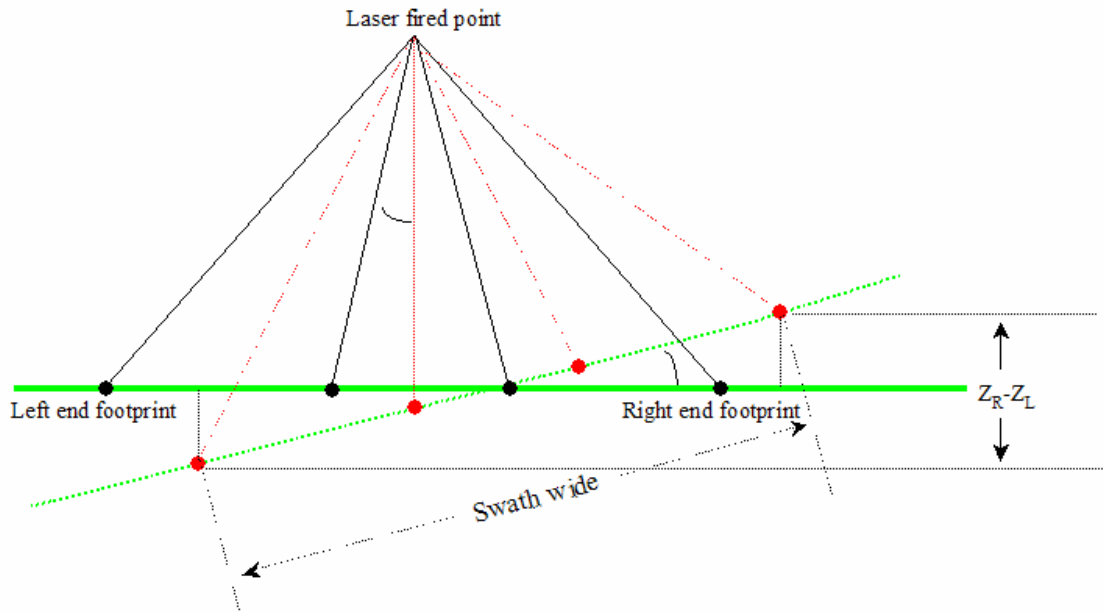
Fig. 5.1. Rolling misalignment deflects the horizontal flat surface and shifts the feature position at the same time

From figure 5.1, we can have the following simple formula:

$$Z_L - Z_R = 2H \tan \theta_{max} \cdot \Delta R \; ; \; \Delta R = \frac{(Z_L - Z_R)}{2H \tan \theta_{max}} \qquad (5\text{-}2)$$

Where $Z_L - Z_R$ is the height difference between left end points and right end points over flat horizontal surface, H is the average flight height over the object, θ_{max} is the maximum scanning angle of the system.

Table 5.1 gives the simulated calculation to show how much the rolling angle deflects the horizontal surface.

Tab.5.1 Rolling angle deflect the horizontal surface

H	200	200	200	200	200
θ_{max}	30	30	30	30	30
ΔR	0	0.5	1	1.5	2.0
$Z_L - Z_R$	0	2.02	4.03	6.05	8.06

5.2.3 Influence of pitch misalignment on laser points

In figure 5.2, the situation shows that the pitching misalignment shifts the feature position mainly along the flight direction, and we can easily get the formula as (5-3) according figure 5.2. Red footprint is the forward flight point influenced by pitching misalignment. Blue point is the backward flight points influenced by pitching misalignment. The forward and backward flight shifts the object in opposite direction (the distance is doubled).
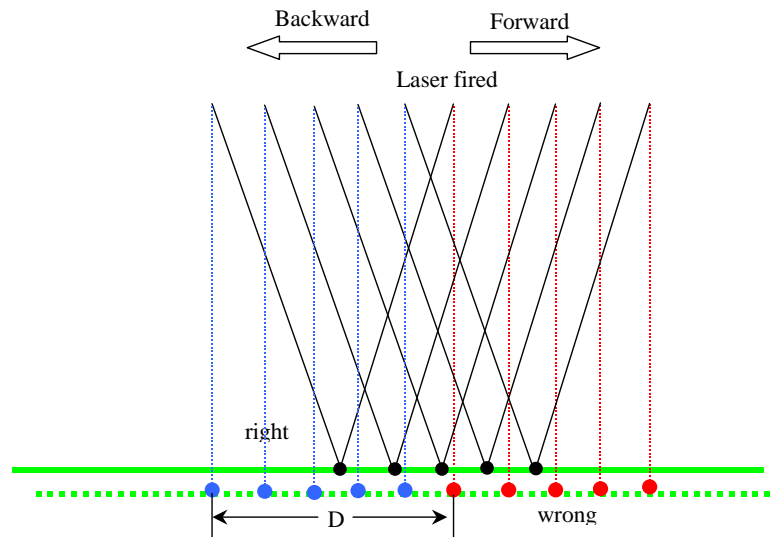

Fig. 5.2. Pitching misalignment shifts the feature position mainly along the flight direction

$$D = 2H \tan \theta_{max} \cdot \Delta P \; ; \quad \Delta P = \frac{D}{2H \tan \theta_{max}} \qquad (5\text{-}3)$$

Where D is the distance between the point clouds forward flight and backward flight, H is the average flight height over the building area, θ_{max} is the maximum scanning angle of the system. Table 5.2 gives the simulated calculation to show how much the pitching angle shift the object position along the flight direction.

Tab.5.2 Pitching angle shift the horizontal position along the flight direction

H	200	200	200	200	200
θ_{max}	30	30	30	30	30
ΔP	0	0.5	1	1.5	2.0
D	0	2.02	4.03	6.05	8.06

Also the heading misalignment shifts the center point (discussed in the next section), but it is possible to design the flights so that it is flown over the object at the same side forward and backward. This will cause the difference (due to heading misalignment) of the two center point positions to almost cancel out. The difference from the pitch misalignment will be doubled at the same time.

5.2.4 Influence of heading misalignment on laser points

Heading misalignment may shift the object position and deform the object. Figure 5.3 demonstrates the heading misalignment influence on lidar point coordinates. Heading misalignment is more difficult to calibrate, since the calibration baseline is not long enough. Here we call the length between the building center point and the flight nadir point the calibration baseline. If the calibration baseline is short, the heading misalignment shift of the feature position is small, and the horizontal coordinates of the laser footprints are not very accurate. However, averaging the point cloud to get the center point position of the object will greatly minimize the horizontal noise from footprints. And if the flight is done forwards and backwards at two sides of the object, the shift will be zoomed in (doubled). In this way heading misalignment is retrieved more accurately.
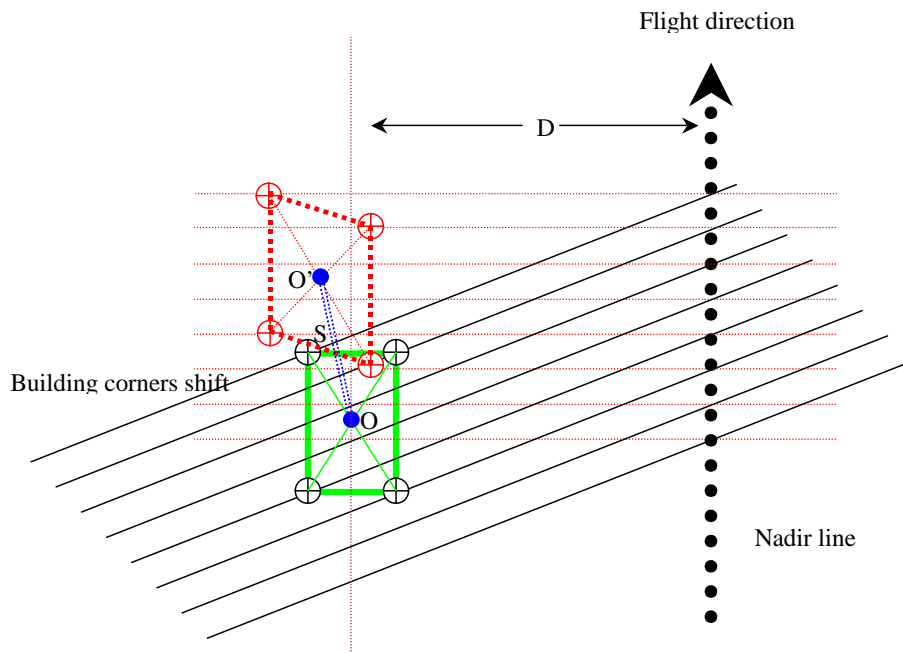

Fig.5.3 Heading misalignment shifts the feature position in both along and across flight direction

$$S = D \cdot \Delta H \ ; \ \Delta H = \frac{S}{D} \qquad (5\text{-}4)$$

Where S is the distance between two center points average from the forward flight and backward flight point clouds, D is the distance between the center point of the selected building and the flight nadir point nearest to the center point.

Tab.5.3 Heading angle shift the horizontal position

D	100	100	100	100	100
ΔH	0	0.5	1	1.5	2.0
S	0	0.873	1.745	2.619	3.492

Table 5.3 gives the simulated calculation to show how much the heading angle shifts the object position.

5.2.5 Strategy to separate the misalignments angle

As discussed above, the influences from the three misalignment angles on lidar footprint mixes up, we have to separate the boresight angles. Only the roll misalignment deflects the flat surface (Fig.5.1), i.e. it is possible to retrieve the roll boresight angle first by investigating the surface reconstructed by laser point clouds on a flat horizontal surface. Then we can correct the roll angle and get a new point cloud data set. The new data set is free of rolling misalignment, only pitch and heading misalignment angle remains. Both misalignments in pitch and heading will make the buildings horizontal position change in flight direction, but position change due to pitch is reversed when the flightpath is reversed (Fig.5.2). If the flight over a building is carried out at nearly the same trajectory in opposite direction the heading misalignment will mostly cancel out. So, by comparing the building center point shift from opposite flight directions, we can retrieve the pitch angle. Generally, the coordinate noise can be lowered by averaging all the points on the building top. In the same way, it is possible to correct the pitch angle and do geolocation again to get new point clouds. The new data set is free of roll and pitch misalignment, now only heading misalignment remains. To retrieve the heading angle, we can use the central point of the building again. If the flight path is not exactly over the top of the building, a heading angle will move the central point of the building away from the true center position which is seen in Figure 5.3. Heading is retrieved using the distance S and distance D in the figure. In this way, when the building is further away from the flights ground track it is easier to make an accurate estimation of heading using the simple formula. I.e. the flight trajectory should be designed in advance to ensure that building is not exactly below the aircraft but that the building is fully covered by the laser scan. Flights from opposite directions on each side of the building is preferred since the difference in position of the building center is maximized, minimizing the need for ground truth for heading retrieval.

5.2.6 Calibration steps

The building top points are mixed up with the ground footprints, so the first step in the calibration process is to do a filtering to extract the building points. The filtering method is a conicoid interpolation as Pfeifer et. al. (1999) introduced. Linear prediction is used for the DTM interpolation. The error distribution of laser scanner heights with reference to the ground surface is no longer a normal distribution but a skew distribution with a strong bias towards off-terrain elevations. The points near the ground are considered to be normally distributed whereas the vegetation and building points have only positive residuals with reference to the ground. In our dataset there is no vegetation., which makes the extraction of the building point cloud very easy. Even in suburban area, it will be possible to select some spot where one can extract the building points from the whole strip dataset.

Even when you got the building points, you don't know the points represented which parts on the building, so we could not compare these points coordinates with the ground truth, e.g. roof corner point positions measured with GPS. Even we can match the lidar points with the true point of the building, the footprint's horizontal coordinates have error with few decimeters. Fortunately, the center point is unique, and we can determine the ground truth of the regular center point, and also we can calculate the center point position of the filtered building point clouds by simple average the coordinates of all building points. By such way, the noise of the

coordinates will be sharply minimized by averaging. So the difference between the calculated center point and the true center point come from the misalignment. Our strategy is to average all points horizontal coordinate as following:

$$\bar{x} = \sum x_i \Big/ N ; \quad \bar{y} = \sum y_i \Big/ N \qquad (5\text{-}5)$$

to got the center point coordinate of the building points clouds, which can minimize or cancel most errors. We can get very accurate center point. The difference between center point and the ground truth of the building center come from the misalignments angle offset. Using the simple formula above, we can retrieve all the boresight directly. In our tests, we select a rectangular building as the calibration reference.

5.3 Airborne lidar system calibration examples

5.3.1 Airborne lidar system description

In the following examples, all laser measurements were done with a scanning lidar of type LMS-Q140i, which provides cross-track scans at a user selectable frequency, with range accuracy better than 5 cm. The laser operates in the near-infrared wavelength band, and has a scan angle of 60 degrees, giving a swath width roughly identical to the flight elevation above the ground.

The Riegl laser scanner (lidar) data was logged as hourly files on a stand-alone laptop computer. The lidar files are time tagged by a 1pps signal from one of airborne GPS receiver, with start time of the scans given by the operator as a file name. Nominally files cover about 1hr of data, at 40 scans/sec and 208 measurements per scan. Files were logged in text or binary (".2dd") formats, yielding a file size of 200-300 MB. Data were written directly on CD's after the flights.

Fig. 5.4 Riegl laser scanner mounted in the aircraft (left) and aircraft hole photographed from under, with scanner mirror, and camera (right).

5.3.2 Calibration example I

The first calibration example is from an airborne lidar survey carried on DOY 144 in 2004. Fig.5.5 is the part of strip near a runway. Buildings used for calibration are seen. Fig. 5.6 shows the filtered building points from the strip.
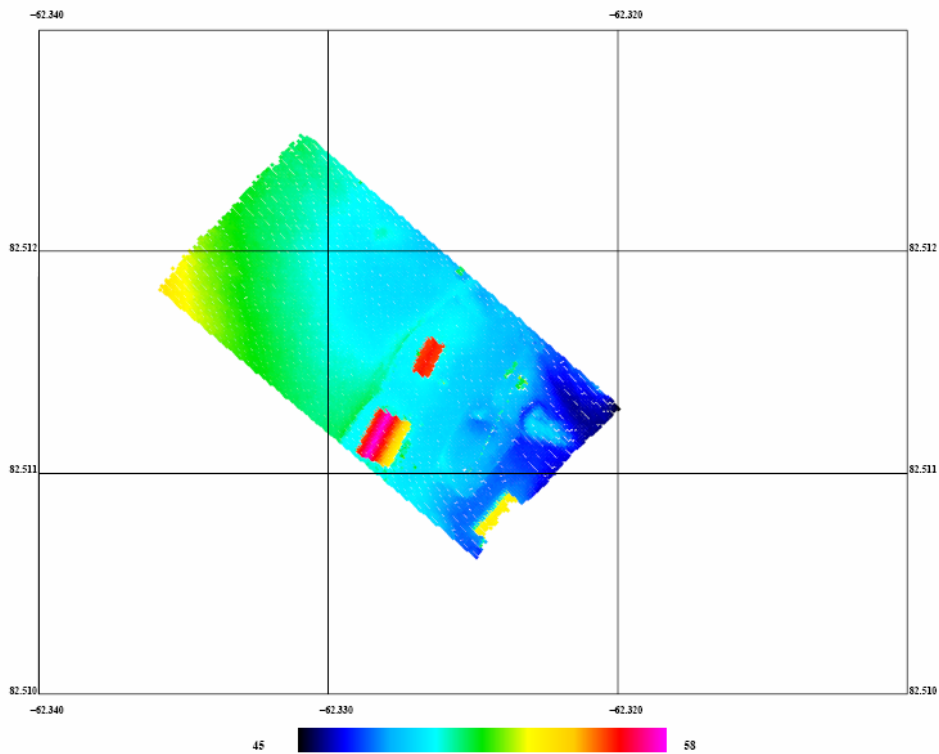

Fig. 5.5 Colored lidar strip with the building used for calibration
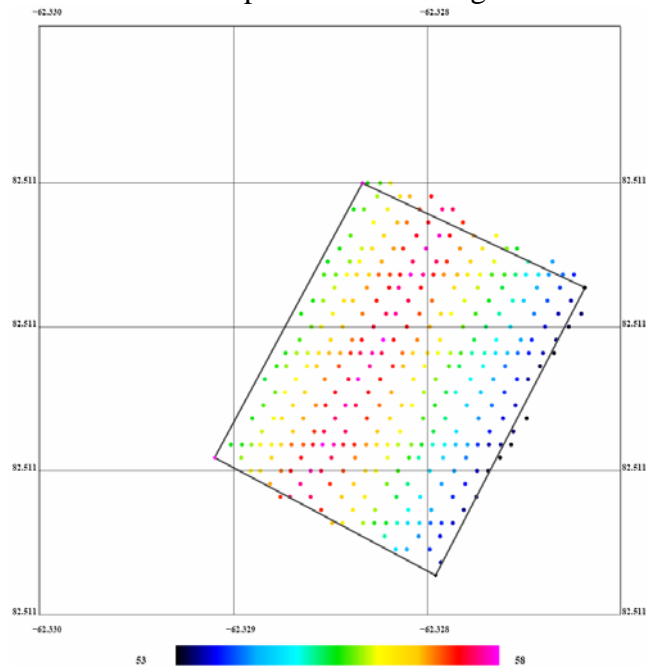
Fig.5.6 Building top laser points extracted from the mixed-up point cloud by filtering

Fig.5.7 gives the comparison of footprints on building top fitting the frame of building top before and after calibration. After calibration, the point clouds of the building fit the building frame very well. The retrieved misalignments values are:

$$\text{pitch0} = 0.35; \quad \text{roll0} = -0.10; \quad \text{hdg0} = -1.00$$
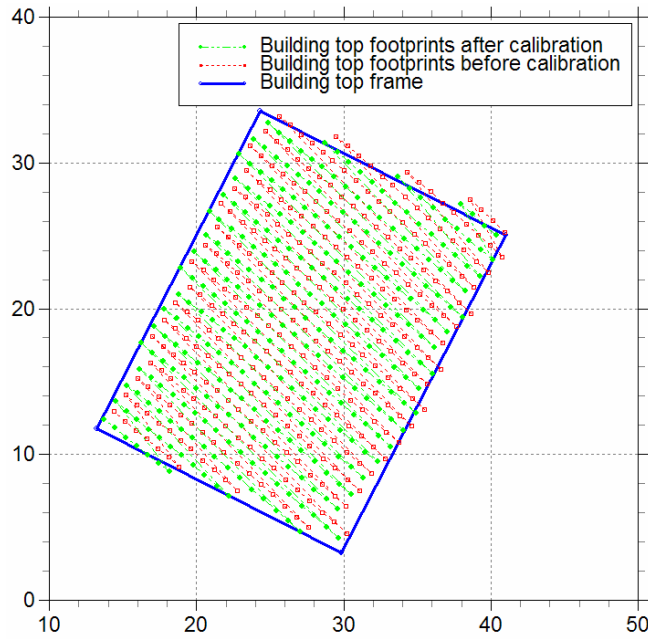
Fig.5.7 Extent of building top footprints fit the building top frame degree before and after calibration

5.3.1 Calibration example II

Example II shows the second urban area where airborne lidar had been carried out in Denmark. Only a part of scan points were on the building for the backward flight. After calibration the footprint fits the building frame.

(a) Before calibration   (b) After calibration
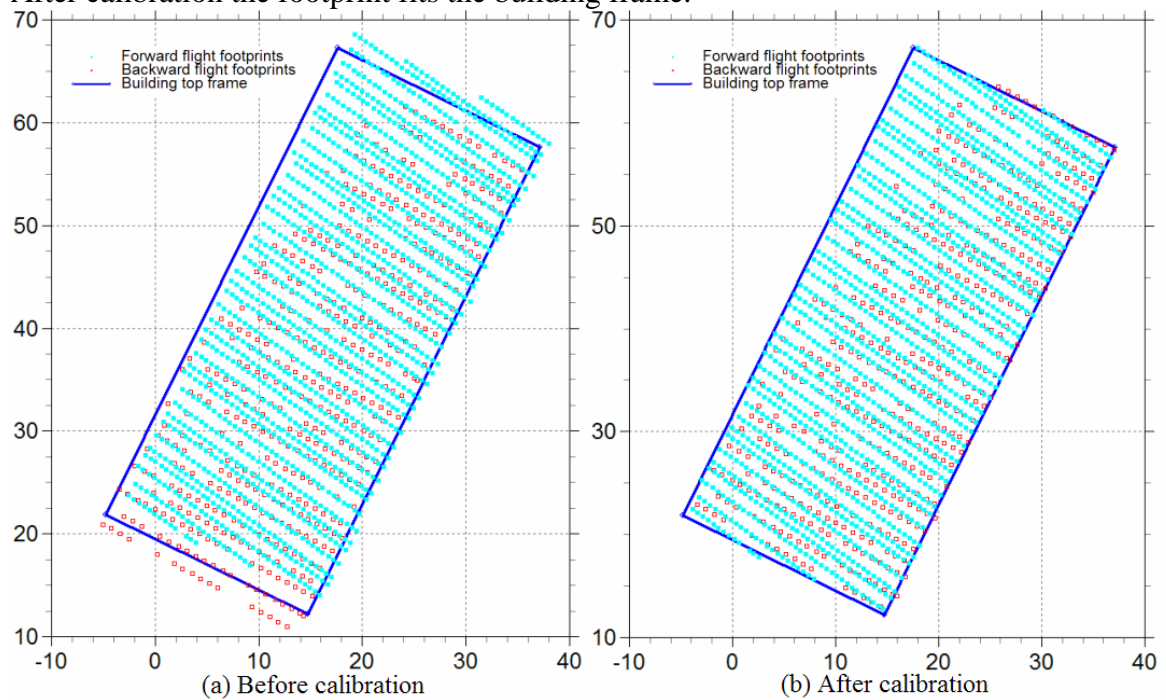
Fig.5.8 Extent of building top footprints misfit the building frame before misalignment calibration and fit the building frame after misalignment calibration

The retrieved misalignments values are:
$$pitch0 = 0.84; \ roll0 = -0.148; \ hdg0 = -0.020$$

5.3.1 Calibration example III

Example III is from the SPICE 2005 campaign. The building was passed four times in order to calibrate and validate the misalignments. Fig 5.9 shows a colored height image of lidar point data from one pass over the building.
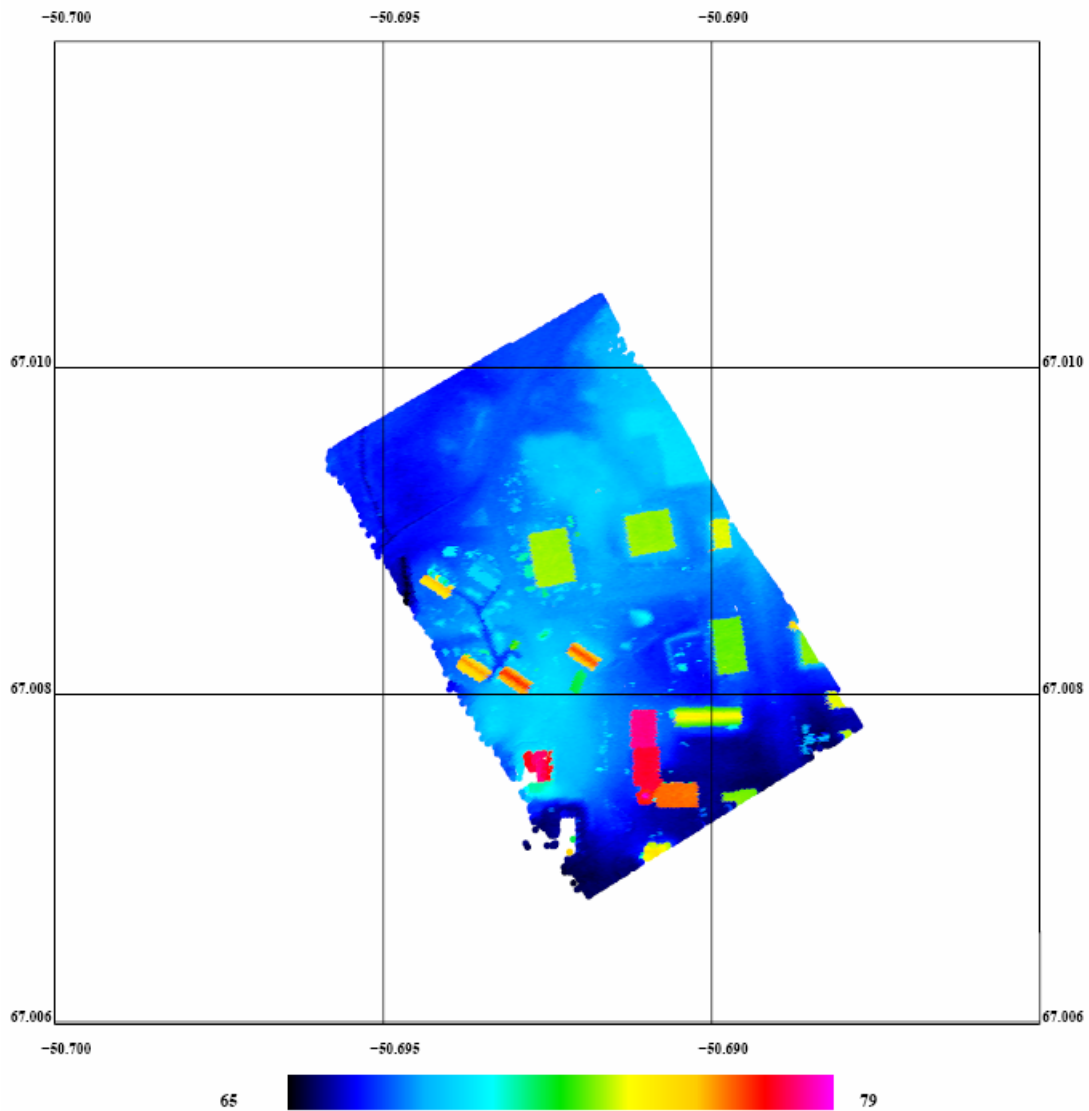

Fig. 5.9 Laser scan over Kangerlussuaq buildings measured by GPS for calibration

The retrieved misalignments values are:

$$pitch0 = 0.25; \quad roll0 = 0.20; \quad hdg0 = -0.05$$

In figure 5.10, before calibration, the lidar points misfit the building frame, and different passes has different directions. In figure 5.11, lidar points on the building from all passes fit the ground truth (building frame) very nicely.

(a) First pass   (b) Second pass

(c) Third pass   (d) Fourth pass

Fig.5.10 Before calibration

(a) First pass   (b) Second pass

(c) Third pass   (d) Fourth pass

Fig.5.11 After calibration
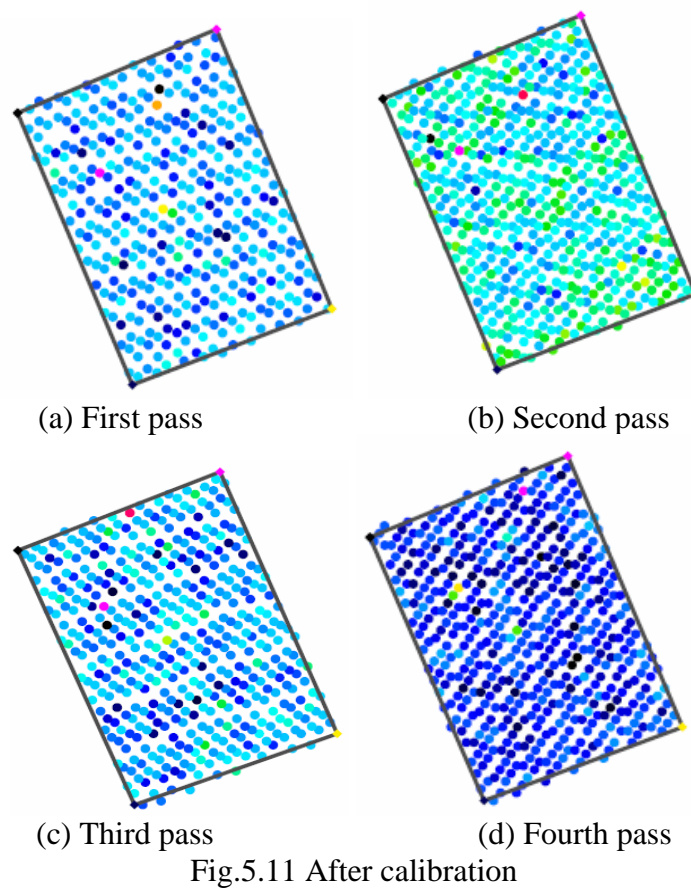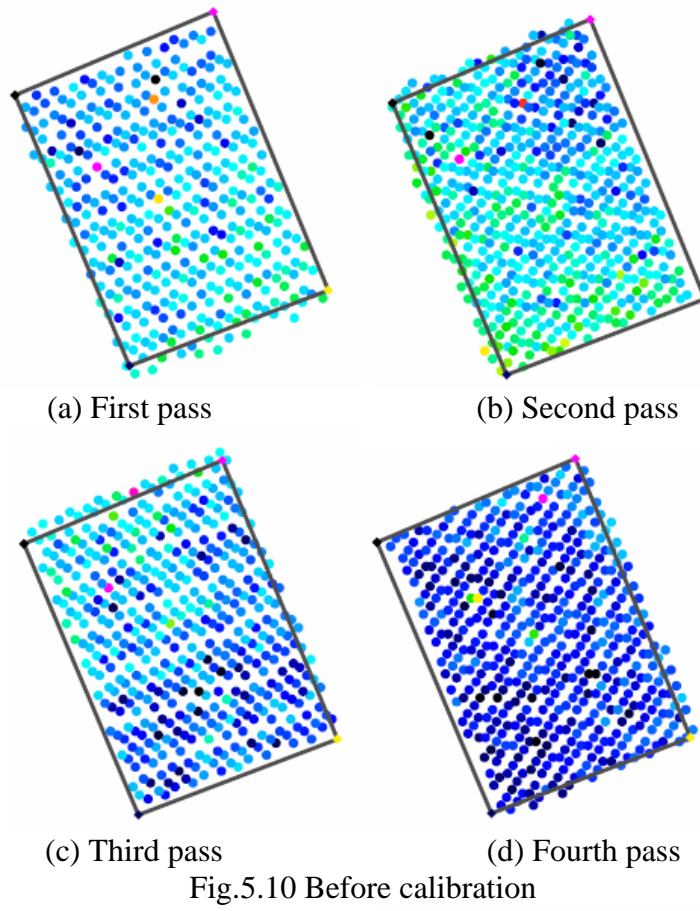
5.4 Discussion

According to the above analysis, the roll misalignment may deflect the horizontal surface and mainly shift the object along the direction vertical to the flight direction. The pitch misalignment shifts the object along the flight direction. Flights passing in opposite directions will double the shift. The calibration flight should be designed in advance to achieve more accurate misalignment angle.

Retrieving the heading offsetdifferent is different. When the forward and backward flights are at the same side of the object, and the flight height and the trajectory overlap, heading misalignment will not double the shift, i.e. both flights results in the same position of the center point of the object. However, when the forward and backward flight are at the opposite sides of the object, the shift will be doubled. Thus, designing flights to pass the object at two different sides, which will result in a more accurate calibration of the heading misalignment.

According to the above analysis, the influence of misalignment angles is bigger when the aircraft flies higher, consequently calibration flights should be made as high as as possible.

6 Conclusions and remarks

6.1 Conclusions and remarks on PPP

Absolute positioning was performed in the static and kinematic mode with the IGS precise orbit and clock (30sec). For the static case, it was conducted by estimating two base stations where the coordinates were determined in the ITRF with reputable GPS software such as, Auto GIPSY or Bernese. The position was determined with a precision of 2~3cm in all three coordinates. Biases to the known coordinate are on the order of 2cm. For PPP mode, the longer the observation, the higher accuracy you can have. One-day PPP solution accuracy can reach few mm level.

This research showed that cm to dm accuracy for kinematic positioning with TriP could be achievable. This accurate absolute positioning can be a powerful technique if the baseline length is too long, if there is no base station near the surveying area, or if the fixed base stations coordinates are not good.

Even though the IGS products are available after different periods of time and with different accuracy, quality control of the data is however questionable. This topic has not been studied although it is crucial in the airborne surveying field since the entire surveying mission depends on the quality of the GPS data. Therefore, it is strongly recommended to study the quality control aspects when implementing the IGS products for airborne surveying applications if the precise point positioning technology is used.

The precise point positioning technique is an alternative way to do long range kinematic positioning when no reference station is available, and almost the same accuracy could be achieved in such case with any dedicated base station. Quality control should be performed when precise point positioning is used in very long range kinematic solutions, because the no integer ambiguities can be fixed in precise point position mode presently, in fact, even using double differenced mode the integer ambiguities also can not be fixed in such cases. On the hand, the tropospheric estimation is also to be investigated more as the aircraft fly over long distance with different atmospheric condition.

6.2 Conclusion and remarks on airborne lidar calibration

The provided new method can be used to determine the boresight misalignment angles automatically. Boresight misalignment can be determined provided building ground truth is available.

The higher the flight height, the easier it is to get more accurate misalignment angles.

The flight pass should be designed before hand to retrieve the misalignment angle offsets. In order to fully retrieve all misalignment angles, it would be better if we could have three times flying over a building.

7 References

Cannon M.E., Schwarz K.P., Wei M. (1992) A consistency test of airborne GPS using multiple monitor stations, Bulletin Géodésique , 66(1): 2-11

Colombo OL, Evans AG (1998) Testing decimeter-level, kinematic, differential GPS over great distances at sea and on land, Proceedings of ION GPS 1998, 15-18 Sept, Nashville, Tennessee, USA, pp 1257-1264

Castleden N., Hu G.R., Abbey, D.A., Weihing D., Ovstedal O., Earls C.J., Featherstone W.E. Recent results of long-range airborne kinematic GPS positioning research at the Western Australian Center for Geodesy, The 2004 International Symposium on GNSS/GPS, Sydney, Australia, 6–8 December 2004

Gao Y, Shen X (2001) Improving ambiguity convergence in carrier phase-based precise point positioning. Proceedings of ION GPS 2001, 11-14 September, Salt Lake City, Utah, USA, pp 1532-1539.

Han, S.(1997) Carrier phase-based long-range GPS kinematic positioning. PhD Dissertation, School of Geomatic Engineering, The University of New South Wales, Sydney, Australia.

Han S., Rizos C. (1999). Sea surface determination using long-range kinematic GPS positioning and Laser Airborne Depth Sounder techniques. Marine Geodesy, 22, 195-203.

Kouba J, Héroux P (2001) Precise Point Positioning using IGS orbit and clock products. GPS Solutions 5(2): 12-28

Mohamed M. R. Mostafa (2005): Precise Airborne GPS Positioning Alternatives for the Aerial Mapping Practice, From Pharaohs to Geoinformatics FIG Working Week 2005 and GSDI-8,Cairo, Egypt, April 16-21, 2005

Schutz B. E.(2002): Laser footprint location(geolocation) and surface profiles, In: Geoscience Laser Altimeter System (GLAS): Algorithm Theoretical Basis Document Version 3.0.

Zumbergre J., Heflin M., Jefferson D., Watkins M., Webb F. (1997): Precise point positioning for the efficient and robust analysis of GPS data from large networks. J. Geophys. Res. 102, 5005-5017.

Zwallya H.J., Schutzb B., Abdalatic W., Abshirea J., Bentleyd C., Brennere A., Buftona J., Deziof J., Hancocka D., Hardinga D., Herringg T., Minsterh B.,Quinng K., Palmi S., Spinhirnea J., Thomasj R. (2002):ICESat's laser measurements of polar ice, atmosphere, ocean, and land. Journal of Geodynamics, 34 405–445

Baltsavias, E.P. (1999). Airborne laser scanning: basic relations and formulas. ISPRS Journal of Photogrammetry & Remote Sensing 54, pp. 199-214.

Filin, S. (2001). Recovery of Systematic Biasaes in Laser Altimeters Using Natural Surfaces.
International Archives of Photogrammetry and Remote Sensing, Vol. XXXIV, Part 3/W4, pp. 85-91.

Krabill, W.B., Wright, C.W., Swift, R.N., Frederick, E.B., Manisade, S.S., Yungel, J.K., Martin, C.F., Sonntag, J.G., Duffy, M., Huislander, W., and Brock, J.C., (2000). Airborne laser mapping of Assateague National Seashore. Photogrammetric Engineering and Remote Sensing, 66, No.1, 65-71.

Kilian, J. (1994): Calibration methods for airborne laser systems. IAPRS, 30, Part 1, 42-46.

Preifer N., Reiter T., Briese C., reiger W. (1999). Interpolation of high quality ground models from laser scanner data in forested areas. International Archives of Photogrammetry and Remote Sensing, ISPRS Workshop, Vol. 32, Part 3-W14, La Jolla, California, 9. -11. November 1999, S. 31 - 36.

Schenk, T.(2001). Modeling and recovering systematic errors in airborne laser scanners. Proceedings of OEEPE workshop on Airborne laserscanning and Interferometric SAR for Detailed digital elevation models, Sweden., Kennert Torlegård(ed)

King, M., 2002. The dynamics of the Amery Ice shelf from a combination of terrestrial and space geodetic data. Ph.d. thesis, University of Tasmania;

K. Keller, S.M. Hvidegaard, R. Forsberg, N.S. Dalå, H.Skourup, L. Stenseng. Airborne Lidar and Radar Measurements over Sea Ice and Inland Ice for Cryosat Validation: CRYOVEX 2003-Final Report, 58 pp, 2004

http://igscb.jpl.nasa.gov/ , 16/8/2005

Technical Report Series

1. Nynne S. Dalå, R. Forsberg, K. Keller, H. Skourup, L. Stenseng and S. M. Hvidegaard: *Airborne Lidar Measurements of Sea Ice North of Greenland and Ellesmere Island 2004. GreenICE/SITHOS/CryoGreen/A76 projects, Final report,* 69 pp., 2005
2. Christian J. Andersen, Nynne S. Dalå, Rene Forsberg, Sine M. Hvidegaard, Kristian Keller: *Airborne Laser Scanning Survey of the Wadden Sea Region, Denmark,* 30 pp., 2005.
3. Sine M. Hvidegaard, A. V. Olesen, R. Forsberg and N. S. Dalå: *Airborne Lidar Measurements of Sea Ice Thickness North of Greenland 2005,* 50 pp., 2006.
4. Xiaohong Zhang: *Precise Point Positioning Evaluation and Airborne Lidar Calibration,* pp. 44, 2005.